5-2012

Cross-Linked PDMS Expansion Due to Submersion in Liquid and Supercritical CO2

Teng Yang
University of Arkansas, Fayetteville

Cross-Linked PDMS Expansion Due to Submersion in Liquid and Supercritical CO2

Cross-Linked PDMS Expansion Due to Submersion in Liquid and Supercritical CO2

A thesis submitted in partial fulfillment
of the requirements for the degree of
Master of Science in Mechanical Engineering

By

Teng Yang
University of Arkansas
Bachelor of Science in Mechanical Engineering, 2010

May 2012
University of Arkansas

Abstract

Characterization of micro/nano-copper particles impregnated Polydimethylsiloxane (PDMS) submersed in supercritical carbon dioxide (scCO2) was studied. The purpose of this investigation was to advance micro-corrosion sensor technology utilizing PDMS and micro-metal particle composite as the sensing element currently under-development. One of the key challenges encountered was the removal of the native oxides inherently existing on the metal particles. Numerous techniques were experimented with to counter this problem at the UA Engineered Micro/Nano Systems Laboratory (EMNSL), with swell-based protocols being identified as the most promising solution. In terms of compatibility to Micro-electro-mechanical Systems (MEMS) fabrication, CO2 is often used in the release of stiction for sensitive microstructures. The experimental method was classified as low temperature techniques (less than 100 degrees Celsius). Commonly, the composite exhibits expansion ratio from 2.5% to 20%, exhibiting more sensitivity to the percentage content of the metal particles, albeit below those reported in literature for pure cross-linked PDMS. The expansion time-constant is found to be on the order of 100 to 1000 seconds.

This thesis is approved for recommendation
to the Graduate Council.

Thesis Director:

_____

Dr. Po-Hao Adam Huang

Thesis Committee:

_____

Dr. Douglas E. Spearot

_____

Dr. Chao-Hung Steve Tung

Thesis Duplication Release

I hereby authorize the University of Arkansas Libraries to duplicate this thesis when needed for research and/or scholarship.

Agreed _____
Teng Yang

Refused _____
Teng Yang

Acknowledgments

I would like to thank my advisor Dr. Huang for his patience, support, and guidance throughout my academic career here at the U of A. I would like to thank Dr. Jerry Wayne King for all the resources and insights provided for this research. I would also like to thank my thesis committee, Dr. Douglas E. Spearot and Dr. Chao-Hung Steve Tung for their patience and time to server on my thesis committee.

I would like to thank all the members of the UA Engineered Micro/Nano Systems Laboratory, John Lee, Jeremy Hutson, Kyle Goldin, Stephanie Clark, and Fen Pan for their help and support.

I would like to thank Drew Fleming for helping with some tough questions in the course of this research.

Lastly I would like to thank my parents, Kui Teng and Zhouqing Yang for supporting me though out my academic career.

Table of Contents

Chapter 1. Introduction

The current goal of the UA EMNSL is to develop a novel micro corrosion sensor that requires the use of PDMS embedded with micro metal particles. This PDMS composite is critical for the sensing element of the sensor under development, and one of the challenges in using micro metal particles is the difficultly in keeping the particles from oxidizing rapidly due to its high surface area to volume ratio. As discussed in the corrosion and corrosion sensing portion of the next chapter, oxidation occurs at the surface of the particle. The result of this large surface area to volume ratio is the rapid oxidation of the particles. There are, of course, a number of ways to keep oxidation from occurring during the sensor fabrication process. One of the more common ways is to keep the process in an oxygen-free environment. This method can be very expensive and also increases the complexity of the entire fabrication process because the oxygen free environment has to be maintained for the entire sensor fabrication processes. Another way is to etch away the oxide on the metal particles after the PDMS-copper composite has already been placed onto the substrate. For cases using copper particles, the oxides can be etched away without significant damage to the particle by using acetic acid [1]. There are attempts of in-situ wet etching of the PDMS-copper composite samples by UA EMNSL but the results were not ideal. The separated oxides did not vacate the PDMS samples completely, and the residual oxides became sediments at the bottom of the sample. The sediments will ultimately affect the electrical resistance across the PDMS composite. The fact that solvents could expand cross-linked polymers, PDMS in particular, has been studied in the past [2] [3] [4]. Then, it is conceivable that if etching could be done when the PDMS composite is in an expanded state, then the oxides could be vacated without leaving any sediment behind.

In order for this newly conceived process to be integrated into the current sensor fabrications process, understanding of this expansion behavior is vital. There are many solvents used in MEMS fabrication process, scCO2 was considered in this study. Among the reasons scCO2 was considered for this study over the other solvents is the ability for the solvent characteristics of scCO2 to be tuned by changing the temperature and pressure. Adjustments in pressure and temperature will change the solubility parameter, diffusion coefficient, and density which should affect the expansion characteristics of the PDMS samples. Another reason CO2 was chosen was its relative inertness. Lastly scCO2 is considered an environmentally clean solvent because it is a naturally present in the atmosphere.

This study will help in the understanding of polymer expansion due to submersion in scCO2 by providing more data in the research area. Literature search on the subject produced three different theories, one is based on solubility parameter, second is based on the diffusion of CO2 and bulk energy, and the third one based on adsorption. It is hoped that with additional data on expansion of PDMS, a more unified theory could be developed in this field.

The expansion of cross-linked PDMS submersed in scCO2 has been studied by multiple groups and their findings have been published. PDMS with embedded metal particles submersed in scCO2 however, has not been studied. Also most PDMS expansion studies do not consider the time to reach expansion equilibrium. After an exhaustive literature search, the amount of expansion and the time to swell to equilibrium is an unknown for the combined PDMS and metal particle composite. In order to use this in-situ etching technique in the sensor fabrication process, the expansion characteristic of the combined PDMS and metal particle composite must be known. The focus of present investigation is to characterize the expansion behavior of cross-

linked PDMS and metal particle composite submersed in scCO2 and to compare results with studies on pure PDMS expansion.

The general expectation for expansion should follow some form of exponential increase (Equation 7) that will reach equilibrium after some characteristic time constant. As pressure of the system increases, the maximum expansion should increase as well. As temperature increases, the PDMS sample should expand more because increases in thermal energy in the system should excite the CO2 molecules, therefore increasing the amount of diffusion into the PDMS composite. The increase in micro copper particles in the sample should diminish expansion because the copper particles should not change volumetrically when submersed in scCO2, and the PDMS portion of the sample will decrease as more copper particles are incorporated into the sample. In summary, the objectives of this research are:

- Pave way for an improved fabrication of MEMS metal polymer composite sensor element.
- Correlate the expansion of PDMS-copper particle composite to CO2 pressure and temperature.
- Correlate PDMS-copper particle composite expansion to particle concentration.
- Determine time constant of the expansion process for both pure PDMS and PDMS-copper particle composite.

Chapter 2. Back Ground Information

This chapter will give some basic ideas and concepts needed to understand the reasoning behind this investigation. The importance of corrosion and corrosion sensing will be discussed first. This is followed by the development of a MEMS-based metal micro-particle composite corrosion sensor being developed at the UA EMNSL. The basic properties of the polymer used in this investigation (PDMS) and the solvent (CO2) also will be discussed. Lastly the current understanding of polymer expansion in solvents is discussed at the end of this chapter.

2.1. Corrosion and Corrosion Sensing

Corrosion is the unintended destruction of metallic material due to electrochemical reactions initiated at the surface of the material. The electrochemical reaction process generally occurs as formation of metal oxides due to a reduction-oxidation reaction. When metal particles lose electrons the oxidation process is initiated. When the electrons react with oxygen forming negative ions of oxygen is the reduction process. In many metals the oxidation process does not stop at the initial surface layer. This process will continue and cause material loss. The loss of material will inevitably cause stress concentrations and structural damage [1].

Corrosion costs in United States are estimated to be about 5% of the national Gross Domestic Product per year, thus, knowing when corrosion has become damaging can be very useful in maintenance and reduction of cost of ownership for infrastructure, transportation vehicles, military hardware, etc. By detecting the source and location of corrosion early, a significant portion of cost of ownership could be saved by avoiding major overhauls and unexpected break downs [5].

There are four types of maintenance strategies. They are corrective, preventative, predictive, and reliability-centered maintenance. Corrective maintenance is centered on repairs and replacement after the damage has occurred. Preventative maintenance is based on regular servicing and replacement regardless of the condition of the structure or part. Predictive maintenance requires active characterization of the status of the structure or part under consideration, making replacement/repairs as needed. Reliability-centered maintenance is conducted on reliability history and risk analysis to improve the other three strategies [6].

For the preventative maintenance method to be effective, corrosion monitoring is vital. In general, there are three types of corrosion monitoring techniques. The first one to be discussed is the offline technique. Generally, this method is conducted with material samples that have a similar composition to that of the material of interest. The change in material dimension or weight loss of the material sample after it is subjected to the same conditions as the infrastructure or equipment in question. This technique can only detect an average rate of corrosion; therefore it can only provide a good guess on the state of corrosion. Another disadvantage is that it generally takes months to produce results, making preventative maintenance difficult. It is also not possible to determine the change in corrosion rate. The second technique is the online technique. This technique uses probes to monitor corrosion and store the corrosion data over time. The advantage of the online technique over the offline technique is that it can detect the rate of corrosion and the data can be collected at a faster rate. The Disadvantage for this technique is that it can only report the corrosion information after corrosion has taken place. The last of the three techniques is the real-time measurement. This technique requires the corrosion information collected by the probe to be transmitted in real-time. The Advantage of this technique over the other two is that it allows for continuous

monitoring [6]. The last two techniques should provide corrosion information in a timely manner for the preventative maintenance method.

2.2. MEMS Corrosion Sensor under Development

The development of a MEMS-based metal micro-particle composite corrosion sensor has been the focus of the research group at the UA EMNSL. The sensor functions by corrosion of metal particles within the composite as corrosive species diffuses into the sensing element. As the particles corrode the corrosion can be quantified by detecting changes, such as its electrical resistance, or electro-chemical noise. The basic operating principles of the metal particle polymer composite corrosion sensor are shown in Figure 1 [6]. As corroding agents diffuse into the polymer composite, oxidation will take place on the surfaces of the metal particles. This process causes changes to the electrical resistance and electro chemical noise within the composite. The changes can be detected by the contact lead on the substrate. This sensor design can potentially provide provide real time corrosion data.

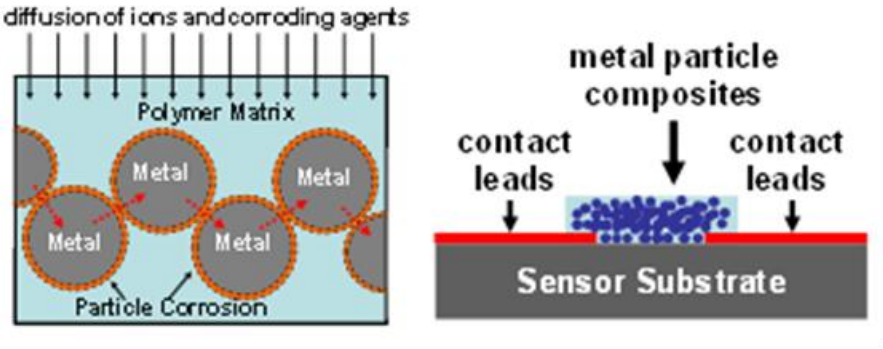

Figure 1: Basic Operation Principles of metal particle poly composite corrosion sensor [6]

The sensor composite can be fabricated using the Direct Polymer Patterning On Substrate Technique (DPPOST) [7]. The process is summarized in Figure 2. The first step is to deposit a thin dissolvable layer (Omincoat^{TM}) on the substrate. Then a mechanically tough sacrificial layer (SU-8, a photo-curable epoxy) is deposited. Both layers war then lithographically patterned with

the desired geometry and etched away. The substrate surface exposed by the pattern is then chemically roughened to enhance bonding between the soft polymer and the substrate. Then the soft polymer is deposited onto the patterned geometry. Lastly the sacrificial layer is removed to expose structures of soft polymer [7].

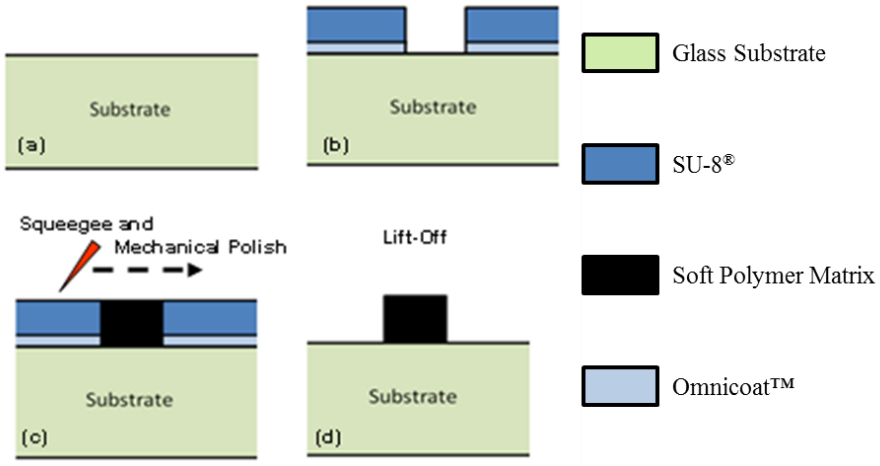

Figure 2: DEPPOST Process [6]

2.3. Polydimethylsiloxane (PDMS)

PDMS is a mineral organic polymer (structure containing carbon and silicon) of the siloxane family (word derived from silicon, oxygen and alkane) [8]. PDMS is a viscous liquid before the introduction of the cross-linking agent. The cross-linked PDMS becomes a viscoelastic material with adjustable mechanical properties depending on the cross-linking process. Cross-linking can take place at room temperature. Because of its commercial availability, chemical stability, low curing temperature, and mechanical flexibility, PDMS is a desirable material for application in MEMS devices, such as those used in microfluidic devices [9] [10]. Cross-linked PDMS sample used in this investigation is shown in Figure 3.

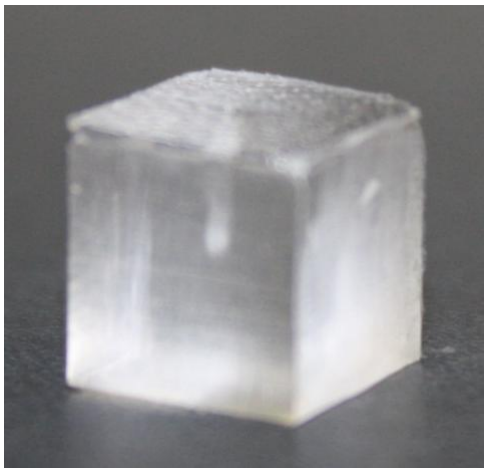

Figure 3: Typical PDMS sample used

The tendency of PDMS to expand when in contact with non-polar solvents should be noted when considering it as material for MEMS fabrication. After exposure to nonpolar solvents, PDMS has the ability to return to its original shape by chemically and/or mechanically desorbing the solvent. However, this relaxation process has to be done gradually to avoid cracking due to excessive local mechanical pressures. The molecular structure of PDMS is a repeating units of $-OSi(CH_3)_2-$ groups. By exposing PDMS to oxygen plasma, the surfaces can become hydrophobic. Oftentimes glass is used as a substrate for mounting MEMS devices. The process involving oxidizing both glass and PDMS surfaces with Oxygen plasma before intimate contact. The resulting chemical bond can be very strong. The expansion of bonded PDMS and glass chips immersed in solvents has been known to break the glass substrate or tear the PDMS. [3]

A property that has been reported to affect expansion of polymers is the solubility parameter. The solubility parameter of PDMS at different temperatures under standard and atmospheric pressure conditions was discussed by Roth [11]. There seems to be a slight decrease in solubility parameters as the temperature increased from 30 C to 90 C. The chain length was a significant factor in determining solubility parameter of PDMS in the same study [11].

2.4. Supercritical Carbon Dioxide (scCO2)

Supercritical Fluids have been used for the last 25 years as an environmentally clean solvent in a variety of technical and chemical processes. One of the advantages of a supercritical fluid is that its solvent strength can be adjusted with pressure and temperature, which enables tuning of the selectivity, degree of extraction, and the degree of loading during an expansion process. In addition, supercritical fluids are soluble in many polymers, often resulting in substantial expansion of the polymer composite, which enhances solute diffusivity [12]. scCO2 has been used to release MEMS structures as a final rinser, due to low surface tension [13]. This method avoids capillary force between the MEMS structures and surround features [13]. scCO2 has been especially attractive due to its moderate critical point at 31.3 C and 7.38 MPa [14]. A possibly problematic characteristic of scCO2 is the large density fluctuations. The density fluctuations are inhomogeneous regions of high and low density. This density fluctuation $<(\Delta N)^2>/<N>$ is defined by the following equation

$$< (\Delta N)^2 > \ < N > = (N \ \ V)_{KT} \, k_b T \qquad \textbf{Equation 1}$$

Where k_b is the Boltzmann constant and T is the thermodynamic temperature, $(N/V)_{KT}$ are known functions of temperature and pressure.

The peak of the density fluctuation forms a ridge on the phase diagram. This density fluctuation ridge passed through the critical point and runs through the supercritical region linearly as seen in Figure 4.

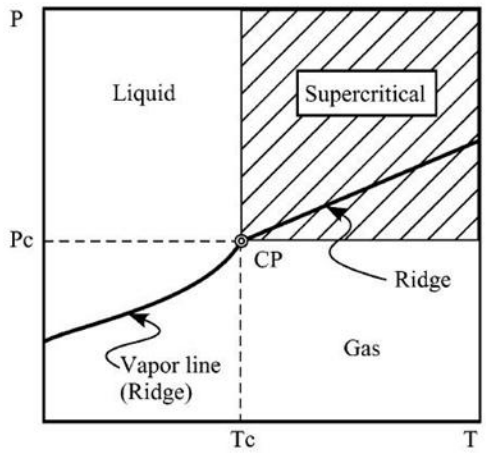

Figure 4: Density Fluctuation Ridge on a phase diamgram. Y-axis is the pressure axis, X-axis is the temerature, Pc is the critical pressure, and Tc is critical temperature [14]

The solubility parameter of CO2 is discussed by Charles M. Hansen. In general the solubility parameter is a function of three different parameters. These parameters are Dispersion Factor, Polar Parameter, and Hydrogen Bonding Parameter. All three parameters increase none-linearly as a function of pressure. This increase was much more evident at higher temperatures. All three parameters decrease as a function of temperature [15].

2.6. Expansion Theories

Three theories were considered for explaining the expansion of PDMS in solvents and, all described the expansion of PDMS well. It is not the scope of this study to investigate the physical-chemical reasons for PDMS swelling, therefore the works from others will be used only as guide for this study.

2.6.1 Theory by Tanaka

Kinetics of expansion of gels has been studied for some time now. Gel is defined as a cross-linked polymer network immersed in a fluid. Analogous result from gel studies in the literature can be used as a guide for the PDMS research reported here.

Theory proposed by Tanaka's states that, "the characteristic time of expansion is proportional to the square of the linear size of the gel and also proportional to the diffusion coefficient of gel network which is defined as $D = E\ \ f$, where *E* is the longitudinal bulk modulus of the network and *f* is the coefficient of friction between the network and the gel fluid" [2]. The time of expansion is directly related to the size of the gel and *D* of the gel network.

The equation characterizing the expansion of gel was derived by Tanaka, Hocker, and Benedeck [16]. A displacement vector u(r,t) is defined as the final displacement of a point in a gel network from its final equilibrium location after the gel is fully expanded meaning the *u* is 0 when *t* has reached an arbitrary infinity. The Equation of Motion (EM) is given by

$$\partial u\ \ \partial t = div\ \sigma\ \ f \qquad \textbf{Equation 3}$$

Where *f* is the friction coefficient between the network and fluid medium and $\boldsymbol{\sigma}$ is the stress tensor of the component of given force along the *k* axis on a unit plane perpendicular to the *i* axis $\boldsymbol{\sigma_{ik}}$ is related to displacement vector u as follows

$$\sigma_{ik} = K\nabla \cdot u\delta_{\ ik} + \ 2\mu(u_{ik} - 1\ \ 3\,\nabla \cdot u\delta_{\ ik}) \qquad \textbf{Equation 4}$$

Where

$$u_{ik} = 1\ \ 2\,(\partial u_k\ \ \partial t_i + \ \partial u_i\ \ \partial t_k)$$

The first term of Equation 4 is the stress caused by volumetric change and the second term is the stress caused by shear deformation. *K* is the bulk modulus of the polymer network and μ is the shear modulus. Equation 4 becomes

$$\partial u\ \ \partial t = \ \frac{K + \mu\ \ 3}{f}\ \ \nabla \times\ \ \nabla \times u\ \ + D_o\nabla^2 u \qquad \textbf{Equation 5}$$

Where

$$D_o = (K + 4\mu\ \ 3)/f$$

In order to solve the EM of gel network, it is necessary to determine the initial condition. Before the gel is submersed into any liquid, it is under uniform stress, so Equation 4 becomes $\sigma_{ik} = \pi_o \delta_{ik}$. π_o is the positive osmotic pressure of the gel. When the gel is submersed in a fluid, the gel will expand until the osmotic pressure becomes zero. If integrated along all directions and assume uniform stress in all direction, the result of the integral would produce a component denoting the final displacement of the gel in equilibrium with the surrounding fluid and a component denoting the change in displacement during the expansion process. With this information, the initial dimensions of the gel can be found. Lastly boundary conditions must also be defined to solve EM of Gel Network. This can be done by knowing that once the gel is submersed in a fluid, the surface of the gel will become free of normal stress. $\sigma_{normal} = 0(on\ all\ surfaces)$.

In principle it is possible to solve the EM of Gel Network. Tanaka and Fillmore solved the equation of spherical gel with 0 shear modulus (μ = 0) to be

$$u\ r,t\ = -6a_o \sum_{n=1}^{\infty} \frac{-1^n}{n\pi} \frac{n\pi\ r\ a\ cos\ n\pi\ r\ a\ - sin\ n\pi\ r\ a}{n\pi\ r\ a^{\ 2}} \times exp(-n^2 t/(a^2\ D))$$

Equation 6

The change in radius of a spherical gel can be expressed as

$$a\ t\ = a_o\ 6\ \pi^2 \quad n^{-2}\, exp\ -n^2\, t\ \tau$$

Equation 7

Where $a\ 0\ /a_o = 1$, n is summation indices, t is time, and τ is the characteristic time of expansion. Expansion experiments were also conducted by Tanaka and Fillmore using polyacrylamide gels submersed in water. The samples were produced by pipetting a mixture of uncross-linked polyacrylamide and cross-linker into paraffin oil. The drops formed will become cross-linked after they rest at the bottom of the paraffin oil container. The experiment was

conducted by dropping the spherical gel into distilled water and the expansion was measured visually under a microscope with a calibrated scale.

The data gathered has been shown to match the theory very well. The typical expansion curve (radius vs time) is shown in Figure 5.

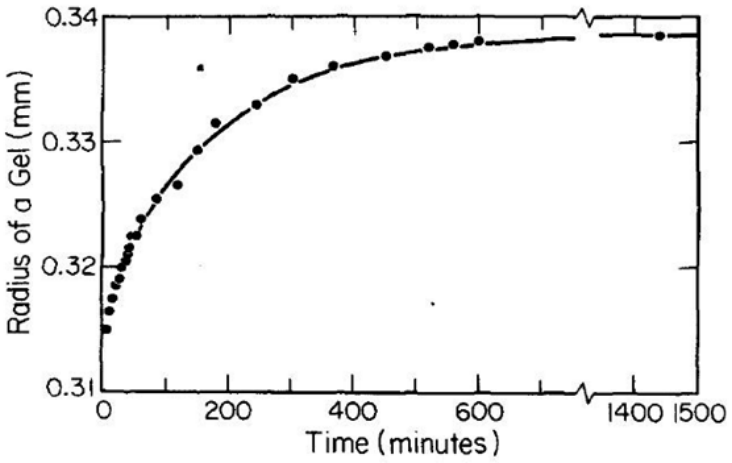

Figure 5 Typical expansion curve observed by Tanaka and group. Radius of the gel sample vs time data points with fitted line [2]

The points on the graph indicates measured points and the solid line is the theoretical prediction of the expansion given by Equation 7. The characteristic time τ is plotted against the squared of the final radius of the spherical gel in Figure 6.

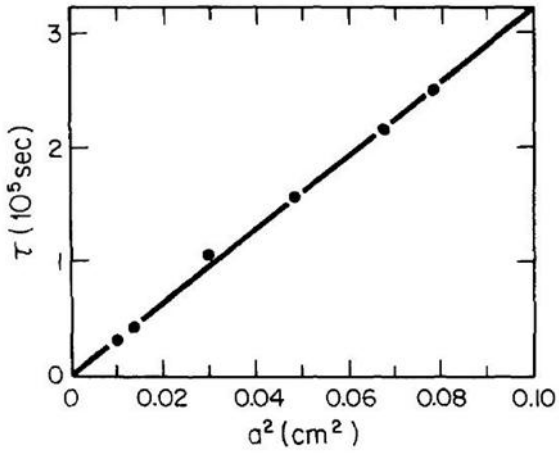

Figure 6: Time Constant observed by Tanaka and group as function of expansion. The time constant vs total expansion of the gel. [16]

Equation 7 only describes expansion kinetics of spherical gels for the case of zero shear modulus. The EM of Gel Network has described the kinetics of expansion of spherical gel. It is important to note that the equation will no longer be valid if the degree of expansion is so large that Hooke's law can no longer describe the elasticity of a gel network. When the sample approaches double its original size due to expansion then the EM must be reformulated.

Tanaka and Li revisited the problem later and devised kinetics of expansion of gel for geometries other than a sphere and with nonzero shear modulus [17]. The zero shear modulus assumption is not accurate to describe the expansion of gels with more complex geometry. It is easy to see the difference in the shear modulus created in Figure 7.

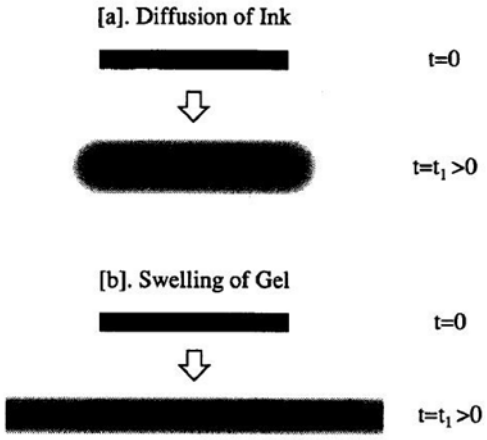

Figure 7 : Difference in diffusion of ink and swelling of gel [2]

The shear modulus is present in gels to keep its original geometry while gel relaxation is the minimization of total shear energy. For asymmetrical geometry this means that a change of dimension in one direction will be coupled with a change in other directions. The total energy of a gel is consists of bulk energy and shear energy. The bulk energy is related to the volume change of the gel which is determined by diffusion. The shear energy is related to the geometry

of the gel. At any instant the shear energy is minimized. The shear energy for a gel of any shape is

$$F_{sh} = \mu \int_V [\, u_{xx} - \frac{T}{3}^{\,2} + (u_{yy} - \frac{T}{3})^2 + (u_{zz} - \frac{T}{3})^2]dV \qquad \textbf{Equation 10}$$

Where

$$T = (u_{xx} + u_{yy} + u_{zz})$$

If the shear modulus μ is not zero and the small changes in geometry of the gel does not change the volume of the gel then

$$\delta F_{sh} = 0 \qquad \textbf{Equation 11}$$

This combined with Equation 5 becomes a much more realistic description of expansion of gels. The introduction of the shear modulus has effectively slowed the rate of diffusion, which is taken into account by a reduced diffusion constant. The reduction factor is related to the dimension in which the diffusion is taking place. For a sphere, diffusion occurs in all three dimensions; therefore the reduction factor is 3/3. For a long cylinder, diffusion occurs in two of the three dimensions; therefore the reduction factor is 2/3. Lastly, for a disc, diffusion only occurs in one of three dimensions, resulting in reduction factor of 1/3.

2.6.1 Theory by Whitesides

Another theory developed by George Whitesides and his group propose that expansion of PDMS is correlated with the solubility parameter, which is based on the cohesive energy density of the material [3]. Cohesive energy density *c* is the energy associated with the intermolecular interactions within a unit volume of material. *c* is the negative of molar internal energy *U*

divided by the molar volume *V*. For materials to be dissolvable, their cohesive energy densities must be similar. For materials such as cross-linked polymers that do not dissolve, solubility parameters can then be used to predict the degree of expansion. The cohesive energy can also be presented as solubility parameters δ or Hildebrad value. The solubility parameter is the squire root of the cohesive energy density

$$\delta = c^{1/2} = (-U \;\; V)^{1/2} \qquad \textbf{Equation 12}$$

The degree of expansion of a polymer can be predicted without knowing any other information. For a binary system, the Hildebrand-Scratchard equation is used to relate the solubility parameter to enthalpy change.

$$\Delta H_m = \; V_m(\delta_1 - \delta_2)^2 \varphi_1 \varphi_2 \qquad \textbf{Equation 13}$$

Where V_m is the volume of the mixture, φ_1 is the volume fraction of solute in the mixture, φ_2 is the volume fraction of the solvent in the mixture, δ_1 and δ_2 is the solubility parameter of solute and solvent. For two parts in the system to be soluble the free energy of mixing must be favorable, that is $\Delta G \; < 0$ and

$$\Delta G_m = \Delta H_m - T\Delta S_m \qquad \textbf{Equation 14}$$

Where

$$\Delta H_m \propto (\delta_p - \delta_s)^2$$

So when ΔH_m is zero, the maximum expansion condition is reached. To validate this theory, expansion data was collected by placing solid PDMS samples in a solvent for 24 hours and the change in length dimensions was measured. The expansion ratio *S* is the ratio of the length of the PDMS sample before submersion divided by the length of the sample after it has

been submersed for 24 hours. The collected data have shown that as solubility parameter of the solvents approaches solubility parameter of PDMS more expansion was detected.

The solubility parameter of PDMS is 7.5cal$^{1/2}$cm$^{-3/2}$ and as the solubility parameter of the solvent get close to that of the PDMS, the expansion ratio generally increased. There are cases where the solubility of the solvents are similar but the expansion ratio was very different. For example, acetone and methylene chloride have the same solubility parameters at 9.9cal$^{1/2}$cm$^{-3/2}$ but the expansion ratio of acetone is 1.06 and methylene chloride is 1.22. This phenomenon can be explained by the difference of the polarity of the solvent. The solubility parameter is also the sum of the dispersion forces, polar forces, and hydrogen bonding forces. Similar solubility parameters do not mean the solvents have the same proportions of the dispersion forces, polar forces, and hydrogen bonding forces. Unfortunately, these values for mentioned forces are not readily available for the solvents in question, but the dipole moment μ is available and it is a representation of the polar contribution. In the example given, methylene chloride has the dipole moment of 1.60D and acetone has the dipole moment of 2.88D. Both methylene chloride and PDMS have lower polar contributions therefore, methylene chloride is more soluble in PDSM than acetone [3].

2.6.3 Theory by Goodman

Study by Goodman comparing carbon dioxide absorption in PDMS has revealed that there are no evidence of reaction products formed between CO2 and PDMS. The study used attenuated total reflectance Fourier transform infrared (ATR-FTIR) spectroscopy to detect gas absorption and to calculate expansion of PDMS. The CO2 absorption in to PDMS results at 50C is shown in Figure 8.

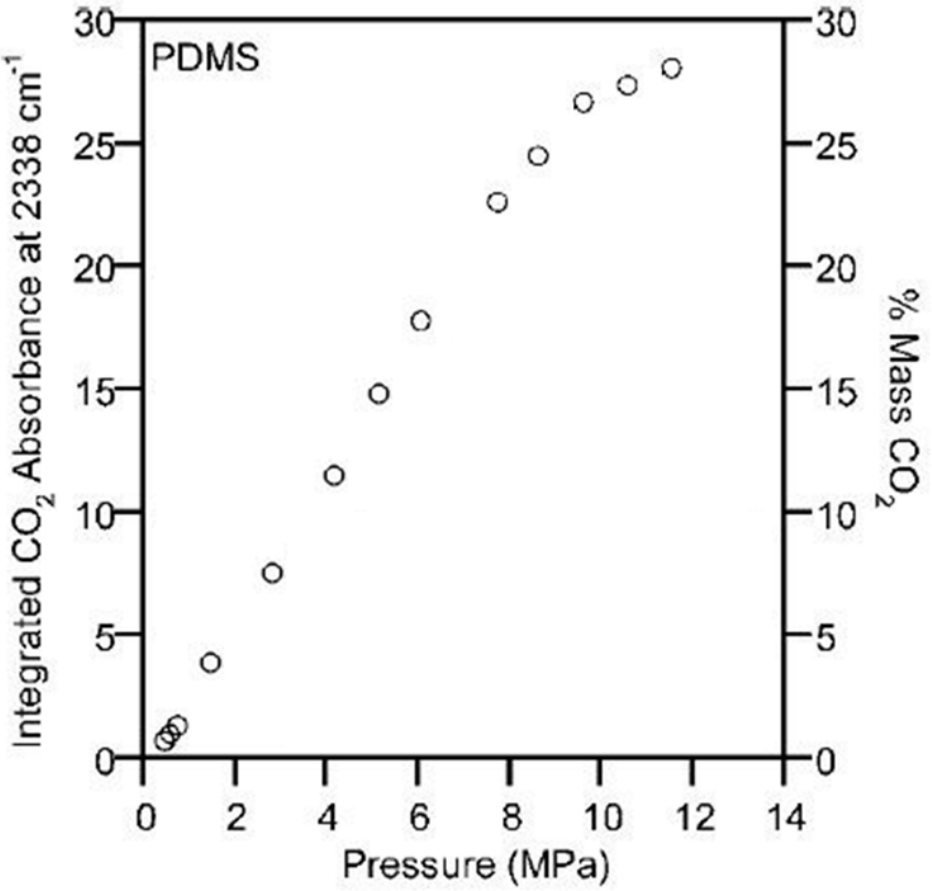

Figure 8: CO2 absorption into PDMS as function of pressure. Mass % adsorbance of CO2 is the y-axis and pressure is the x-axis. Absorbance is becoming more nonlinear at 10 MPa [4]

The data was taken when the adsorption band no longer changed with time. This is defined as the equilibrium state, and the PDMS reached this equilibrium within minutes. Expansion of the PDMS is directly correlated to absorbance before and after exposure of CO2.

$$\%S = [(A^o \ \ A) - 1] * 100 \qquad \textbf{Equation 2}$$

A^o is the net absorbance of PDMS before CO2 exposer and A is the net absorbance of PDMS during Exposure to CO2. The % expansion calculated by using net PDMS absorbance is plotted in Figure 9 [4].

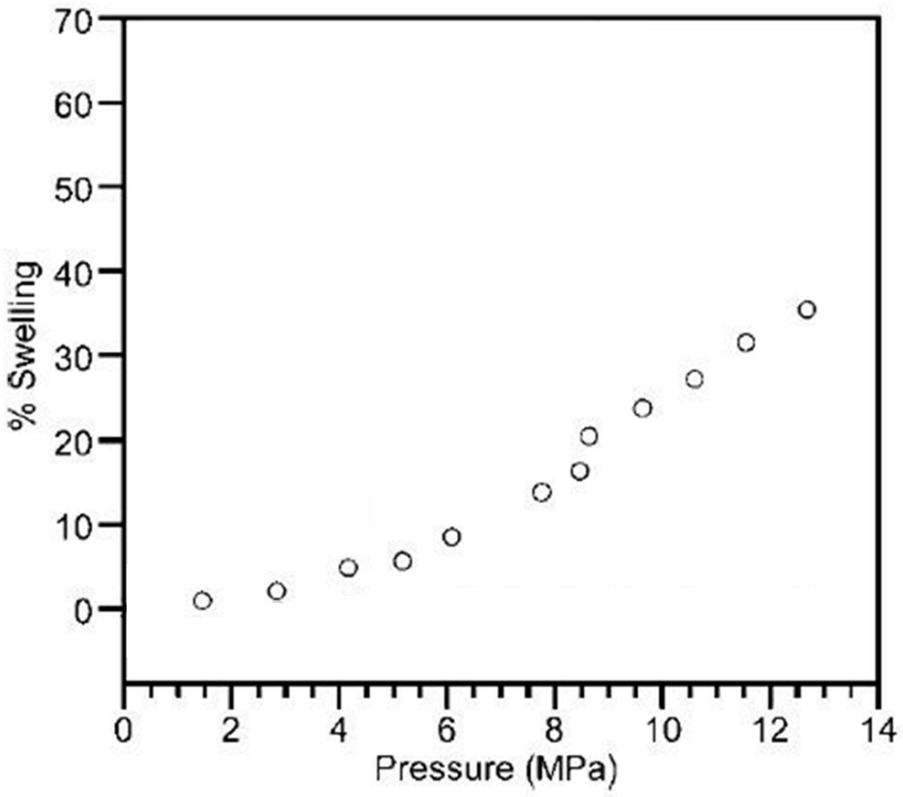

Figure 9: PDMS expansion calculate by using equation 2 is pressented here as expansion(swelling) vs pressure [4]

Chapter 3. Experimental Setup

This chapter will discuss the experimental setup and the rationale behind each step of the experimental setup.

3.1. Experimental Design

The number of experiments and combination of temperature, pressure, and PDMS to copper ratio to be experimented with was carefully considered. It was known from previous works by the UA EMNSL that the saturation of copper in PDMS is around 80 weight % copper [1]. It was decided that the region closer to the saturation was more interesting to the development of the corrosion sensor, so a finer step was chosen closer to 80 wt% Copper. The variations of PDMS to copper ratio are 20 wt%, 30 wt%, 40 wt%, 60 wt%, 80 wt%, and 100 wt%. which correlates to approximately 64.49 vol%, 75.69 vol%, 82.89 vol%, 91.59 vol%, 96.67vol%, and 100 vol%. the volume percentage was calculated with the assumption of particle density of 7.01 g/cm^3 and PDMS density of 0.965 g/cm^3.

The critical point for CO2 is 304.2 K (31.05 C) and 73.8 bar (1070.38 Psi) with slight discrepancies between different studies [18]. The discrepancies were smaller than the accuracy achievable by the equipment used. It was also decided that that the subcritical region is worth investigating. Thus pressure range from 1000 Psi (6.98MPa) to 3000 Psi (20.68MPa) with 500 psi (3.45MPa) intervals was set for this investigation. 1000 Psi (6.98MPa) is just under the supercritical pressure for CO2, and 3000 Psi (20.68MPa) is what the syringe pump can be pressurized to without refilling the syringe.

The temperature range was determined to be 40 C to 80 C with 10 degrees increments. The temperature control set up is only capable of heating the apparatus and the sensitivity of the

temperature control unit cannot maintain temperatures close to room temperature. The temperature step was dictated by limited temperature control issue discussed in the temperature control section later. Because of the limited time allowed, no experiment was repeated unless error has been spotted during the experiential process. The resulting experimental matrix is shown in Table 1.

Table 1: Experimental Matrix

	PDMS to Metal Particle Ratio wt% (vol%)	Pressure (Psi)	Temperature (C)
	20 (64.49)	1000	40
	30 (75.69)	1500	50
	40 (82.89)	2000	60
	60 (91.59)	2500	70
	80 (96.67)	3000	80
	100 (100)		
Variables	6	5	5
Total Exprements	150		

3.2. PDMS Samples

The PDMS samples where made under a fume hood inside a clean room located at EMNSL. The mass of the PDMS, cross-linker, and copper particle used for every batch of sample made was recorded in a lab book.

3.2.1. Sample Mold

Initial attempts at making PDMS samples were utilized molds formed by the rapid prototype 3D printer. The mold consisted of ABS plastic layered on top of each other. The first iteration mold was designed to produce 1 x 1 x 0.1 in. sheets of PDMS that will be cut later by a

knife which is shown on the right side in Figure 10. This mold was not used due to a meniscus-shaped curvature on the free –surface of the molded PDMS. Attempts at over filling the mold resulted in a convex meniscus, and the extra PDMS could be removed, using a Xacto® knife, from the convex meniscus without damaging the top surface of the PDMS sheet.

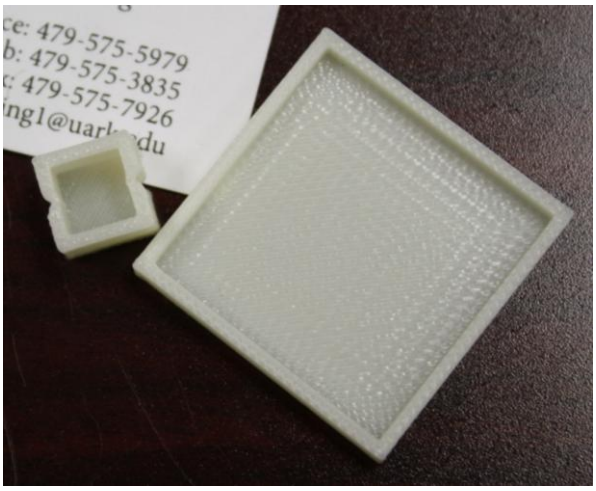

Figure 10: First (right) and second (left) iteration mold

Because of the meniscus issue, it was decided that a sacrificial mold designed to produce one 0.25 x 0.25 x 0.25 in. sample per mold should be attempted, as shown on the left side in Figure 10. Wedges were designed into the sides of the mold in order to facilitate mold release. In theory, when the mold was physically deformed the thinnest part at the wedge would break, thus breaking the mold and releasing the sample. Because of the 3D printer resolution the designed wedge protruded into the sample space resulting in wedges on the sample surface as can be, seen in Figure 11.

Figure 11: Samples produced by second iteration mold

Another version of the 3D printed sacrificial mold was attempted. This time, the design was changed to have taps instead of wedges to separate the mold from the sample. After the PDMS sample was cured, two out of the five sides of the mold can be broken off to release the sample. This version of the mold was used to produce samples for the preliminary experiments. The success rate of this mold was also low. Primary failures of this mold were the bubbles left inside the mold after curing.

It was discovered, after the preliminary experiments, that the 3D printed mold does not have the resolution to produce samples with smooth sides required for the experiment. When the sample was placed in the view cell, the image acquired would have blurred edges, and this could not be over came by the edge finding software. The blurred edges were caused by ridges left from each layer of the 3D print process. These ridges are transferred onto the PDMS samples after the sample was released from the mold. Textures were left on all five sides where the mold came in contact with the sample. The ridges cannot be removed due to the inherent 3D printing process.

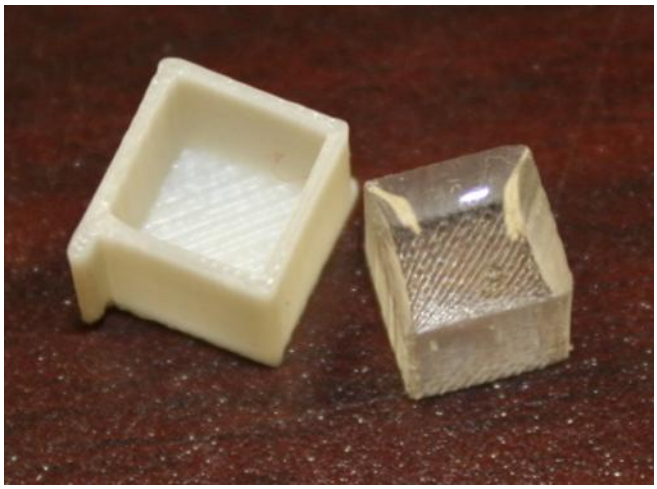

Figure 12: Final 3D printed PDMS mold and sample produced. Notice the texture on the sample.

The 3D printed molds were abandoned and a machined aluminum mold was attempted. The first iteration was a 0.25 in. thick 1 in. wide aluminum strip with 0.25 in cut outs on the outside edge. This was then sandwiched in between two 0.25 in. thick 1 in. wide aluminums strips. The assembly was bolted together with 1/4-20 bolts and nuts with appropriate washers to avoid deforming the aluminum strips.

Figure 13: First iteration of the aluminum mold for the PDMS test sample

The sample was formed inside the 0.25 x 0.25 x 0.25 in. space. When the curing process was completed, the bolts are removed, and the samples can be easily released from the mold.

The resulting samples have smooth sides and clearly defined edges and corners. The PDMS sample required preexisting holes to mount to the view cell apparatus. This requirement is discussed in the view cell apparatus section. These holes were provided by a 3D printed strip with pegs that is strapped onto the top of the mold by zip ties when the sample cures. It took multiple attempts to 3D print in different orientations to get this strip with pegs that will not break. The completed final version of the mold is shown in Figure 14. Two such molds were produce to increase the speed of PDMS sample production.

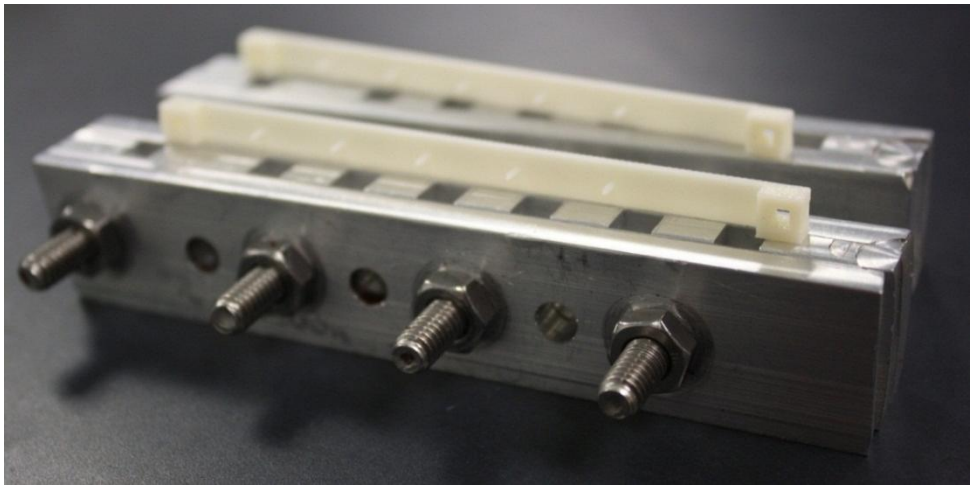

Figure 14: Mold used for fabricating all of the samples used in this thesis work

3.2.2. PDMS Mixing, Degassing, and Curing

A Sygard 184 Silicone elastomer kit was purchased from Dow Corning and used for all experiment. The kit came with two separate parts, one part PDMS and one part cross-linker. The PDMS component is a heavy and viscous substance. The cross-linker has a much lighter, less viscous liquid. The specific chemical makeup and most physical properties of the PDMS and cross-linker are stated in the data sheet. The cross-linked PDMS was produced following the instructions provided by Dow Corning. The instruction from Dow Corning stated that the PDMS

base should be mixed thoroughly with the cross-linker at a 10 to 1 weight ratio to produce cross-linked PDMS.

The copper particles were purchased from Alfa Aesar. They were ±325 mesh particles with diameter varying from 8 to 11 microns. The particles were not kept in an oxygen free environment; therefore they have already been oxidized to an unknown degree. These particles are the primary health concern for this investigation, due to inhalation hazards. All transferring of the particle from original packaging to the daily use packaging was done under the fume hood.

Trials were done to determine the most effective method for mixing, degassing, and curing of the PDMS sample. The first trials were done with thoroughly mixed PDMS and cross-linker mixed with copper particles at predetermined mass ratios. The curing time was set at 24 hours at room temperature as instructed by the Sygard 184 Silicone elastomer kit manual. The results were not satisfactory, the copper particles were not distributed evenly, and there were air bubbles formed within the sample. Over 90% of the samples were not useable. The reason for the uneven distribution of the copper particles was determined to be settling of the heavier copper particle to the bottom of the sample. The air bubble in the sample was due to the bubbles introduced during the mixing process.

Subsequent trials were conducted to address these issues. A pre-curing process was introduced to increase the viscosity of the PDMS to help keep the copper particles from settling to the bottom of the sample. An elevated temperature final curing step was also used to shorten the curing process. A shortened curing time should reduce the time for the particles to sediment. Several temperature and time combination from the Figure 15 [1] were tried. It was determined that per-curing at 60 C for 20min and then another 30min of final curing worked well. Elevated

temperature is provided by a Cincinnati Sub-Zero Micro Climate Control oven shown in Figure 17.

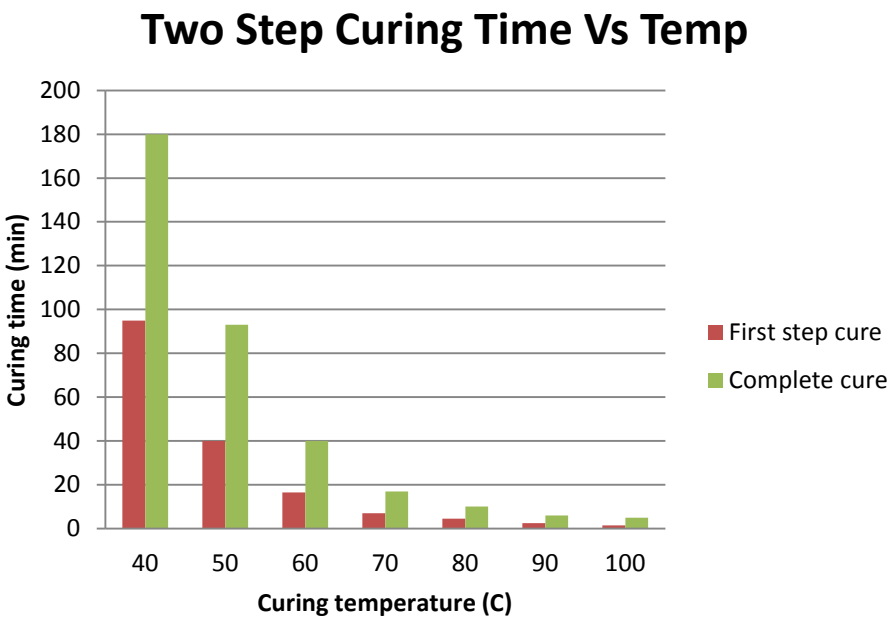

Figure 15: PDMS curing time as a function of temperature [1]

A degassing process was introduced to eliminate the air bubbles. The first trials used a converted container modified from a plastic food preservation box. This system pulled a maximum vacuumed of 60 Psi (21.5 Torr) with only one degassing step, which was done before the final curing at 60C. The resulting samples were not perfectly cube due to material unintentionally removed during the degassing process. As the vacuum pulled gases from the sample mixture, bubble form within the sample mold and rise to the top of the mold. These bubbles carry sample mixture to the surface and expel the mixture out of the mold resulting in reduced sample mixture inside the mold. Multiple degassing steps were taken so that the mold could be refilled in between each degassing step. Another new degassing system (from the Parylen coater camber model PDS 2010 manufactured by Specialty Coating System) that could achieve vacuum of single digit Torrs was also was used to replace the modified plastic food

preservation box, see Figure 16. The new vacuum also had a more reliable seal which provided more consistent processing between different batches of sample. The much higher vacuum allowed for a more complete degassing process.

Figure 16: Parylen coater camber model PDS 2010 manufactured by Specialty Coating System used to degas the samples.

The final process consist of four degassing steps each lasting about five minutes. The first degassing step was after the PDMS and the copper particle was mixed together, before it was placed in the mold. The second degassing step was done after the mold has been filled. Excess PDMS and copper particle mixture was degassed along with the filled mold. The mold was refilled with the excess mixture after the degassing step. This was repeated one more time. The fourth degassing step was not followed by a refilling step. The mold was placed in the Cincinnati Sub-Zero Micro Climate control oven for the final curing process. Once the mold

was removed from the oven, it was allowed to sit over night before samples were released from the mold to ensure consistency for the cross-linking process.

Figure 17: Cincinnati Sub-Zero Micro Climate Control oven

3.3. View Cell Apparatus

The original intent of the experimental set up was to visually observe scCO2 as pressure and temperature increase. This apparatus was originally designed and built by an undergraduate research student working for Dr. Jerry Wayne King of the University of Arkansas, Department of Chemical Engineering. The setup needed to be upgraded and modified for the purpose of this investigation. The original set up programing did was programed inadequately, image acquisition was done as video, temperature and pressure readings was not recorded in a text file. The program language used was not compatible with the image processing program. The view cell was does not have any mechanism to keep a PDMS sample in place for the image acquisition of the PDMS sample be consistent. Noisy raw temperature signal was filtered by digitally

averaging the sampled data. The resulting temperature data can be plus or minus 2 degrees from the set temperature and with high frequency variations up to 5 degrees. The modifications and upgrades will have to address all the issues mentioned. The completed view cell set up after modification is shown in Figure 18.

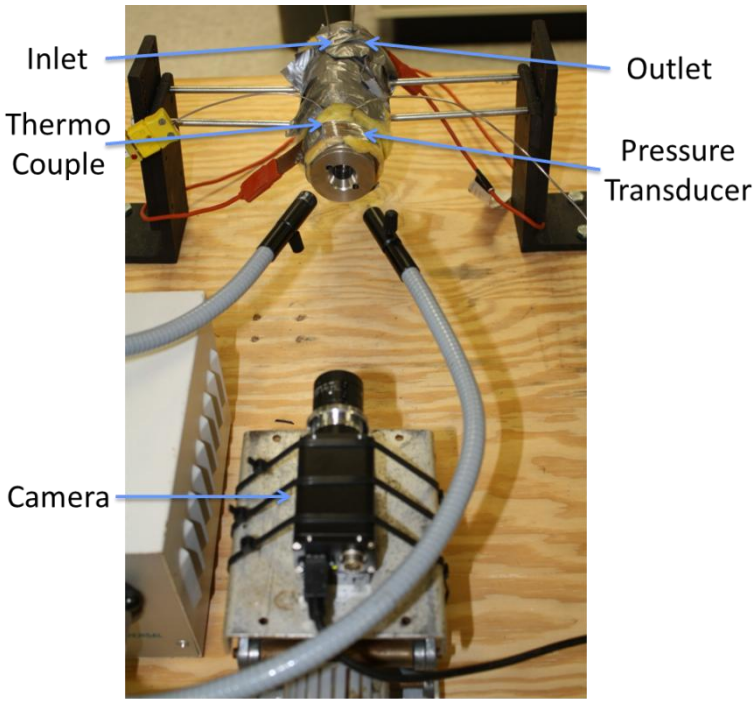

Figure 18: The completed view cell setup

3.3.1. View Cell

The original purpose of the apparatus was for visual examination of scCO2 therefore it was mostly ready for the use of this investigation. The view cell is a stainless steel tube 6.875 in. long. The inside and outside diameter was measured to be 0.75 in. and 2.0 in. respectively. There are four tapped holes for 8 mm fittings along the outside of the tube in a 2 x 2 pattern. These tapped holes are for the thermal couple, pressure transducer, CO2 inlet, and CO2 outlet. The ends of the tube are capped off with 1.5 in diameter threaded caps. The cap encapsulates a

circular sapphire window, with dimensions 1.0 in. diameter 0.275 in. thick, between the cap and the tube. Buna N-213 O-rings were used to maintain a pressure seal around the sapphire windows. The overall volume inside is about 3 in^3. The view cell is rated to 15000 Psi, but the maximum pressure attempted successfully was 5000 Psi during trial runs.

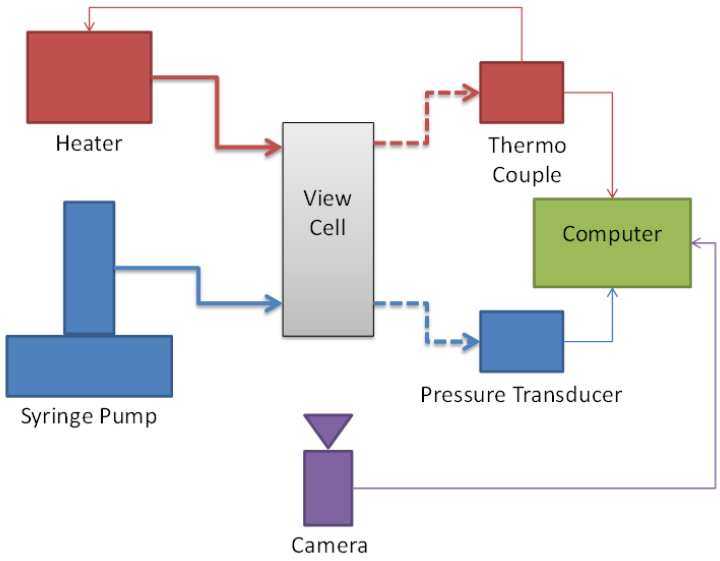

Figure 19: View cell setup schematic

It was decided that the view cell can safely operate at the elevated temperature and pressure so therefore there was no need to modify it.

3.3.2. PDMS Holder

As stated before, the view cell used was not designed originally to have PDMS samples inside. The first trials of pressurizing the view cell with a sample inside were done by leaving a sample in the view cell without any support or bracing. The results of the trials was that the sample washed around in the view cell and the image acquisition device (camera) had no way of determining the before and after condition of the sample. Thus, a mounting mechanism was needed to keep the sample stationary in the view cell so that the entire expansion process could

be captured by the camera. This device must not restrict the sample from dilating while the inside of the view cell must be left unaltered after the experiments are done. A few variations of the sample holder were attempted before a design was finalized. Because the inside of the view cell is smooth, it was difficult to mount any devices inside without changing the geometry inside the view cell. A device resembling a gallows that sat on two horizontal plates (Figure 20) was first considered. But it has few major draw backs. The first of the drawbacks was that it took up too much space inside the view cell where the space was already limited. The second drawback was that it has to be made very small which will make the fabrication process challenging and time consuming. Third, the horizontal plate base would not be stable enough to maintain the same orientation for the duration of the experiment.

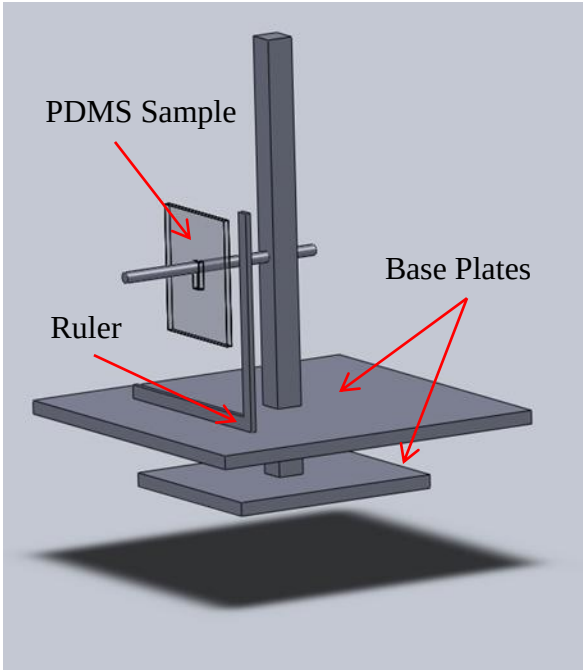

Figure 20: PDMS holder first iteration design

It was decided that a tube with the same outside diameter as the inside diameter of the view cell should provide a much better base to mount the holder than the horizontal flat plates.

This tube design will not damage the inside of the view cell. A aluminum was chosen for this application because it is easy to machine and it has a favorable thermal expansion coefficient, the stainless steel has a coefficient of thermal expansion of around 15 K^{-1} while aluminum's is around 25 K^{-1} [19]. As temperature increased the aluminum will expand faster than stainless steel, which will result in a friction fit between the stainless steel view cell and the sample holder during the experiment. The holder can be released when the view cell apparatus cools back down to room temperature. An aluminum tube with inside and outside diameters of 0.438 in. and 0.875 in. respectively, was chosen as the starting material. The outside diameter was worked down to 0.76 in. and by sanding away a small amount of the material at a time to have a close fit with the view cell. The inside diameter was not big enough to accommodate the 0.25 in. PDMS sample sufficiently. The concern was that if the sample had an unexpected level of expansion it would come in contact with the side of this tube making the experiment invalid. The inside diameter was therefore enlarged to 0.6 in.

On the first iteration of this tubular sample holder, a gold vector pin used for pinted circuit boards was press fitted into a hole drilled on the side of the aluminum tube see Figure 21. The pin fitted inside the whole left in the PDMS sample. After a series of experiments it was discovered that the gold pin did not keep the sample from rotating about self during the pressurization process. To prevent rotations of the sample during the experiments, a small screw was press fitted into the aluminum tube instead, as shown in Figure 22. The screw provided more surface area for friction between the aluminum/head of the screw contact and also for PDMS/thread contact. The resulting set up performed well and was used for the remainder of the experiments.

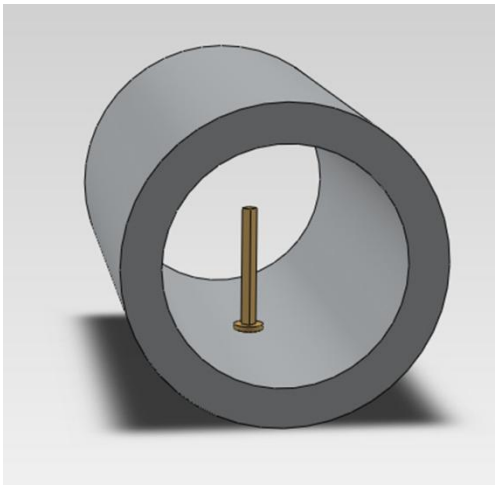

Figure 21: PDMS holder with gold pin

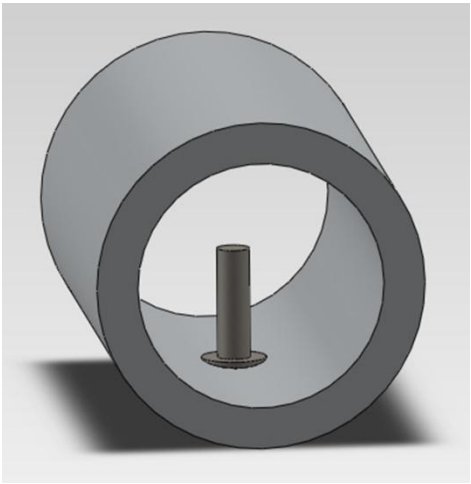

Figure 22: PDMS holder with the screw

3.3.3. Pressure Control

ISCO 260D syringe pump controlled by ISCO D Series controller was used to supply the CO2 at the pressures required for the experiments. The liquid CO2 supply tank was used to fill the ISCO pump is at a normal pressure of 600 Psi. The ISCO 260D pump has a capacity for 266 ml (16.23 in^3) and a maximum pressure of 7500 Psi, which is enough to pressurize the view cell to the desired pressures for this investigation. In order to pressurize the view cell rapidly, a cooling process was incorporated at the CO2 intake of the ISCO 260D syringe pump. The

cooling process was provided by a Neslab cooling bath, with the bath temperature set to 0 C. Although the CO2 temperature at entry of the view cell is not instrumented, it can be assumed that it is close to 0 C. However, the pressure inside the view cell was rarely the set pressure due to several reasons. The fluctuation in density inherent in pressurized CO2 discuses in the back ground section could be one of the reasons. Another reason could be the sensitivity of the syringe pump pressure transducer, and the reaction speed of the syringe pump. These two factors cannot be eliminated with the equipment available to this investigation. The last reason was the pressure transducer used to monitor the pressure within the view cell giving false readings. This was the least likely scenario because the transducer was new and calibrated before being used in this setup.

3.3.4 Temperature Control

In this research only heat can be actively applied to the view cell while, cooling relies on natural dissipation down to the lab's ambient temperature, normally at 23C. the thermocouple provided the feedback for the thermo controller to regulate the power supplied to the Omega flux heating tape thus controlling the heat input into the system. The temperature controller was an Omega Engineering, Inc. type CN5001k2 thermo controller. A type-K thermocouple manufactured by Omega was used to sense the temperature within the view cell through one of the four 8 mm tapped holes on the view cell. It did not protrude in to the inner diameter of the view cell in order to allow the sample holder to slide into the view cell freely. The heating tape was wrapped around the view cell, and a layer of insulation was applied on top of the heating tape to improve efficiency. To reach the designated temperature quickly for the test volume inside the view cell, the view cell was heated to the test temperature before the pressurized CO2

was introduced. By experience, the temperature control system was only accurate within +/-2 C around the region of operation for this investigation.

3.4. Pressure, Temperature, and Image Data Acquisition

A Sentra 3100S15KPT2T9 pressure transducer's was connected to the inside of the view cell via another one of the four 8 mm tapped holes. The pressure transducer will output 0 V to 10 V corresponding to 0 psi to 15000 psi. This signal was then inputted in to the computer via the National Instruments SCB-68 Shielded I/O Connector Block for Data Acquisition Devices with 68-Pin Connectors and the National Instruments 6036E 200kS/s, 16-bit, 16-Analog-Input Multifunction Data Acquisition card.

Thermocouples work by having a pair of different metallic wires joined at one end which produces thermoelectric voltage at the open end with magnitude corresponding to the temperature difference at both ends [20]. The thermocouple poses a greater challenge than the pressure transducer because of the noise issue. The unfiltered raw signal resulted in high frequency fluctuations of 10 degrees. A capacitor-based low pass filter was used to partial filter the high frequency noise while digital data averaging was used to limit it with in a 2 degree C fluctuation. It has been determined that the noise was introduced by the temperature controller do to its alternation current injection into the heating tape.

Image data acquisition was performed by a Scout machine vision camera manufactured by Basler. The original view cell set up was intended only to view the near the sapphire window. Additional lenses were required provide the required depth of focus in the view ell where the cubed sample resides. . A combination of a 25 mm lens and a 10 mm focal length extender purchased from Edmund Optics was employed to provide the necessary viewing distance and focus required for this investigation. The camera set up was then fixed to a scissor jack. This

was done to provide stability so the vibrations from the work bench do not produce inconsistent data from one moment to the next during the experiment; also to ensure that the camera remain at the same location so that the setup was consistent for all experiments. The camera was then connected to the computer through its FirewireII interface. The camera was the only experimental parameter the computer controlled. The pressure was controlled by the syringe pump and the pump controller not coupled with the computer. Temperature was controlled separately by the thermo-controller.

LabView programing was used for the machine vision, pressure, and temperature data acquisition. The program was built around a "while loop per image acquisition". Pictures of the sample in the view cell were taken at about two per second. For every loop a unique millisecond based time stamp was generated and used to name the corresponding image file. The time stamp is also stored in the first column of a designated "Data.txt" file (essentially a data log file). The pressure data from that same millisecond was saved to the second column of "Data.txt" file after the voltage result was converted to pressure value in Psi. Similarly, the temperature data was saved on to the third column of the "Data.txt" file after the voltage value was converted to temperature in Celsius. The picture was saved in the same folder as the "Data.txt" file. This was done until the user stops the loop. The LabView VI and the block diagram are presented in Appendix A.

3.5. LabView Image Processing

LabView Vision Assistant software was used aid in the development of a LabView Virtual Instrument (VI) program used to post process the recorded data, screen capture of the VI during processing is shown in Figure 23 .

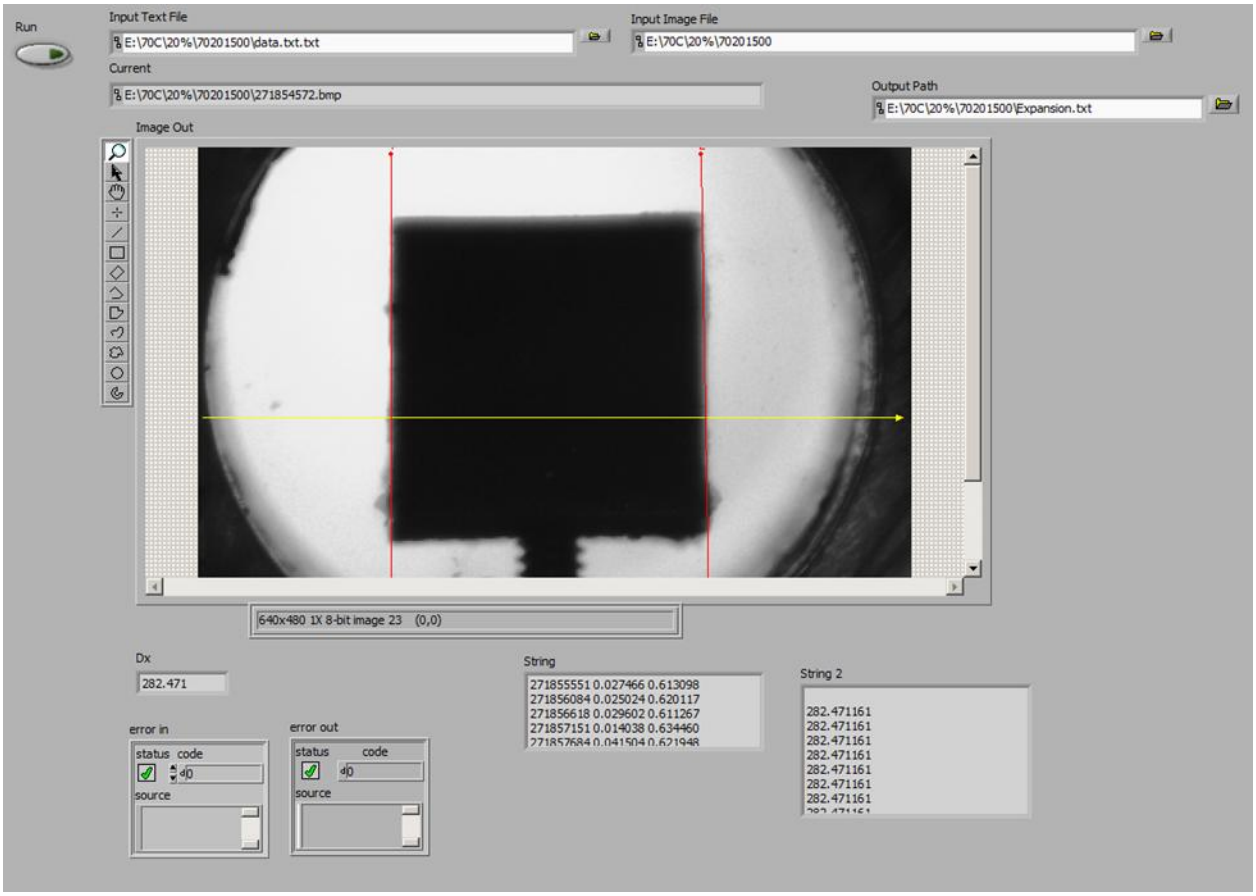

Figure 23: Post processing VI screen capture.

First the post processing VI imports the image file name from the first column of the "Data.txt" file. This was done by inputting the folder location where the image files and the "Data.txt" file was saved before the post processing VI is initiated. Once the image file name was constructed the VI then proceed to import the image file.

LabView's built in visual processing VI could detect changes in brightness and color to find edges of objects in the image. This capability was used to scan for the edges of the PDMS sample within the image; from left to right for the left edge of the sample, and then a repeated scan from right to left of the right edge of the sample in the image. The edges found were not always perfectly vertical. So the width values for the top most point and the bottom most point of each edge line were averaged. The resulting difference from the two averages was then used as

the width of the PDMS sample at the time the image was taken. Figure 24 is a flow chart of the process, and it also includes a typical edge finding iteration by the LabVeiw VI.

The result was then written in to the fist column of a text file specified by the user before the VI loop was initiated. To be consistent all new file was named “expansion.txt”. This process repeated untill all millisecond time stamped value in the “Data.txt” file is processed. Every time a new image is processed the result is written to the next slot down of the “expansion.txt” file to avoid overwriting the previous iteration of the loop. The LabeView VI and block diagram is located in Appendix B

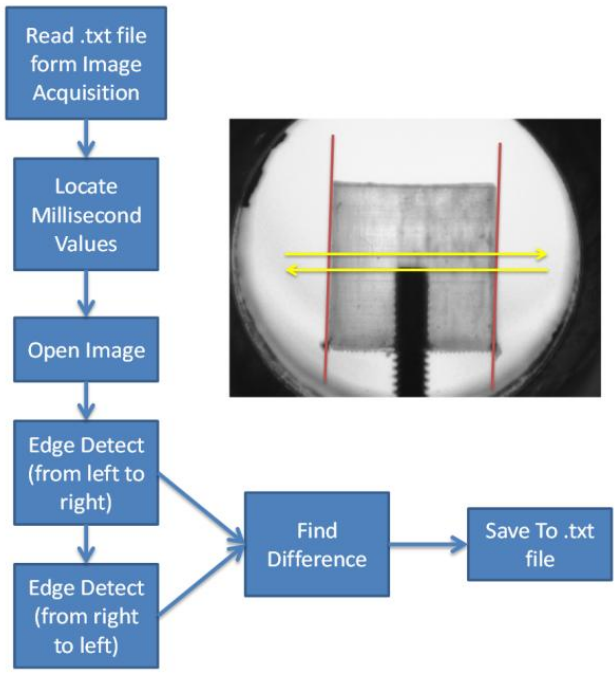

Figure 24: Flow chart of the LabView VI describing one iteration of the edge finding process

3.6. Expansion vs Time Curve

After the data Images has been process by the LabView VI, the results from “expansion.txt” and “Data.txt” was imported to an excel file given a name unique to each

experiment. The file name was created with temperature, sample ratio, and pressure. So the experiment involving a 20% PDMS sample submersed in 1500Psi and 40C scCO2 would have the file name 40201500.xlsx. This was done so that the file can be easily recognizable and to avoid confusion.

In order for time to start at zero, all millisecond time stamp values were subtracted by the first millisecond time stamp value. The result of this operation was that all the time stamps became time elapsed from the start of the experiment in milliseconds. The resulting expansion vs time data is then plotted. The initial width of the sample in pixels was extracted from the average values from the 60^{th} image to 120^{th} image. This correlates to a time span of about 30 seconds starting around 30 seconds from initial data acquisition. The fully expanded width was extracted from the average value from the 6000^{th} to 6061^{th} image this also correlates to a time span of about 30 seconds staring around 3199 second from the start of the experiment. This point was chosen because it is far beyond the steady state points from the initial trial experiments. This was done for all experiments by importing text files into an excel template file which is then renamed with the naming convention described before. It is very important that every file follow the same format in order for the MATLAB program described later to work properly. The initial width and the expanded width was then collected for all experiments conducted under the same temperature to produce the expansion data, typical results resemble Figure 25. Excel unfortunately do not have an adequate line fitting function to extrapolate the time constant from data of this particular investigation, so MATLAB was employed for such function.

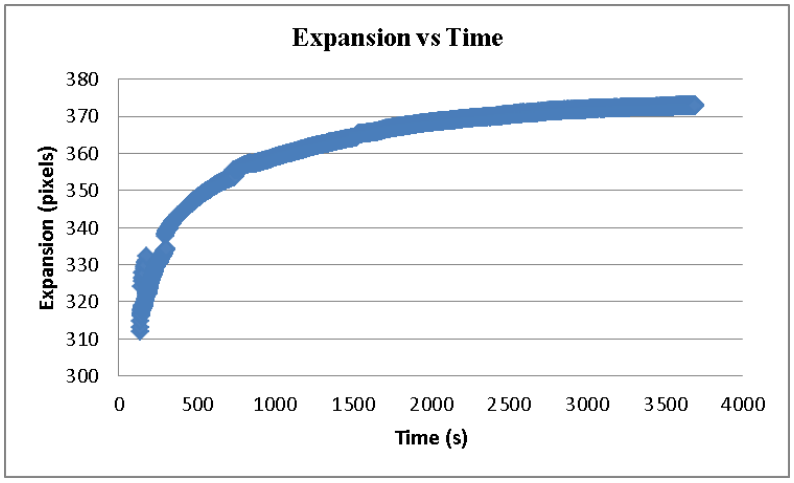

Figure 25: Typical expansion vs time expansion plotted after the data has been imported to MS Excel

3.7. MATLAB Curve Fitting

Curve fitting was used to find the time constant for each experiment. After the LabView process, the data was imported into the excel file with specific naming convention. This unique naming convention described in the previous section will allow the MATLAB Curve Fitting process to be automated. The code that performed the automated curve fitting process was discussed next, see code in Appendix C.

Three layered 'For Loops' was used to construct the excel file name from which the data was imported. The first loop will determine the first variable in the naming convention from a list of possible temperature values provided. The second loop determines the second variable in the naming convention from a list of PDMS ratio values. The last loop determines the third which was determined in the same manner as the first two. The excel file name is then constructed from the three variables determined by the layered "For Loop". With the name of the file and the directory of the file, MATLAB can now import the data from the appropriate column and row from the appointed excel file.

The last loop was where the curve fitting algorithm is placed. The code for the curve fitting algorithm is mostly generated by MATLAB as an .m file. One of the functions of MATLAB is that it can self-generate .m files to complete the process that the user has recently accomplished in MATLAB. So the curve fitting tool (MATLAB code "cftool") was used to find an appropriate curve to fit the data collected. It was decided that the first ten summations from a modified Equation 7 [2] should be used.

$$\Delta a\ t\ =\ d\qquad n^{-2}\ exp\ -n^2 bt\ +c \qquad \textbf{Equation 15}$$

The constants d, b, c and the R value are printed to the command window of MATLAB after each curve fit. The constant 'd' corresponds to $\Delta a_o\ 6\ \pi^2$ in Equation 7, constant 'b' corresponds to $1/\tau$ in Equation 7, and constant 'c' corresponds an correction in the y-axis because the data does not start form (0,0). Different smoothing methods, thresholds, and initial guesses were experimented with. This process was then turned into an .m file, the particular lines of code involving the parameter of the curve fitting and the lines used in the curve fitting was then placed in the last loop of the automated curve fitting .m file.

The resulting curve fit was then plotted over the data for each of the curve fit performed. Typical plot was shown in Figure 25. The figure is plotted to check that the fitting was done reasonably. The constants and R values were then copied and pasted into another excel file. This was done because the three for loops have produced a three dimensional array. To write a code that will write the information to an excel file or a text file automatically would take much longer than to perform the process manually. After the resulting d, b, c, coefficients and R were saved to the appropriate excel file where the inverse of b was calculated, the result was the time constant for each curve fit. The time constant was defined as the time it took the sample to reach

its equilibrium state under the temperature and pressure conditions within the view cell. The .m file is in Appendix C.

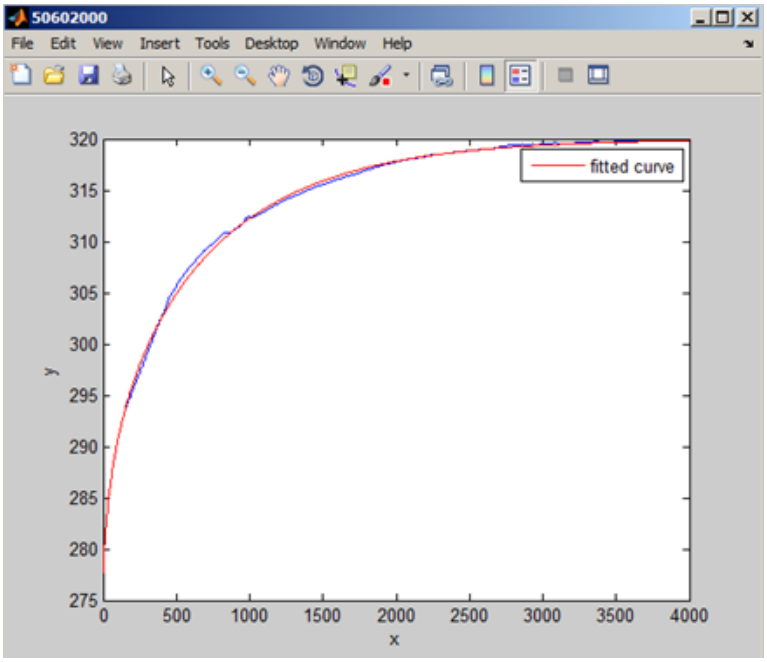

Figure 26: Typical curve fit of the expansion curve. The red line is the fitted curve and the blue line is the data.

3.8. View Cell Experimental Procedures

All view cell experiments were carried out in room 2540 at the engineering research center. First step in conducting the expansion experiments was to make sure the equipment are in working order and all temperature control system are set at the desired temperature. The CO2 reservoir was also checked and opened. If this was the first experiment of the day the syringe pump was tested by pressurizing up to 3000 Psi. The Neslab cooler was turned on and set to 0 C and the heating tape was plugged in and the thermo controller was set to the desired temperature. It will take about an hour for the cooler to reach the set temperature. The second step was to weigh the sample and record the information, this step was taken to determine if significant amount of copper has left the sample during the expansion process. The third step was to mount

the sample onto the sample holder. It was very important to make sure the sample was mounted in such a way that it will present one of the surfaces to the camera parallel with the lens. The forth step was to place the PDMS holder inside the view cell and be pushed to the camera end of the view cell. The fifth step was to check the setup with the camera by initiating the camera control software in LabView program. The sixth step was to close the view cell, enclosing the sample inside. The seventh step was to initiate the data acquisition program. The syringe pump was activated in the eighth step about a minute after the data acquisition program was initiated. Data gathered during this time was used to establish the pre-expansion width of the sample. When the syringe pump starts to pressurize, the valve between the syringe pump and the view cell was opened and the valve for pressure release on the view cell was closed. The experiment was left running for the next hour. When the experiment was over, the valve between the syringe pump and the view cell was closed, syringe pump was turned off, and the pressure relive valve was opened. The data acquisition program was left on during this in hopes of capturing the decompression process. Majority of the data gathered during the decompression process was inconsistent because the relive valve could not be controlled consistently. The sample was then removed from the view cell and weighed three times, immediately after it's removed from the view cell, an hour after the experiment and 2-24 hour after leaving the view cell. The used sample was then placed in storage.

Chapter 4. Data

4.1. Expansion and Pressure

The expansion vs pressure plots is presented in this section. Every plot in this section is consists of expansion and pressure data for all six PDMS and copper particle ratio at a given temperature. As expected, pressure and total expansion forms a positive correlation. This correlation however, was not a linear relationship for lower temperatures but becomes more linear as temperature increases. As shown in Figure 27 and Figure 28 the expansion plateaued after 2500 Psi (17.24MPa). From Figure 29 to Figure 31 the expansion increases linearly as pressure increase.

Maximum expansion generally occurred at 3000 Psi (20.68 MPa) for all temperature and PDMS ratio except for 40 C and 50 C cases. The maximum expansion for 40 C data set occurred when pressure was around 2500 Psi (17.24MPa) at 22.4% this is also the greatest expansion observed from all the experiments conducted. The minimal expansion occurred at 1000 Psi (6.89 MPa) for all temperature and PDMS concentration. As pressure increase, the difference in the magnitude of expansion between different concentrations of PDMS increases. Difference between 100wt% PDMS and 20wt% PDMS for expansion under 1000 Psi (6.98 MPa) is only around 3% for all temperature ranges. On the other hand difference between 100wt% PDMS and 20wt% PDMS for expansion under 3000 Psi (20.68 MPa) vary from 5% to 10% as temperature increases.

50 C data have shown an anomaly in that the 80wt% PDMS samples have expanded more than 100wt% PDMS sample. This is anomaly do not make physical sense, when the sample has higher PDMS content it should expand more because copper should not contribute to

the expansion. It is highly likely that this anomaly was caused by human error. But without repeating the experiments it is not possible to determine the cause with certainty.

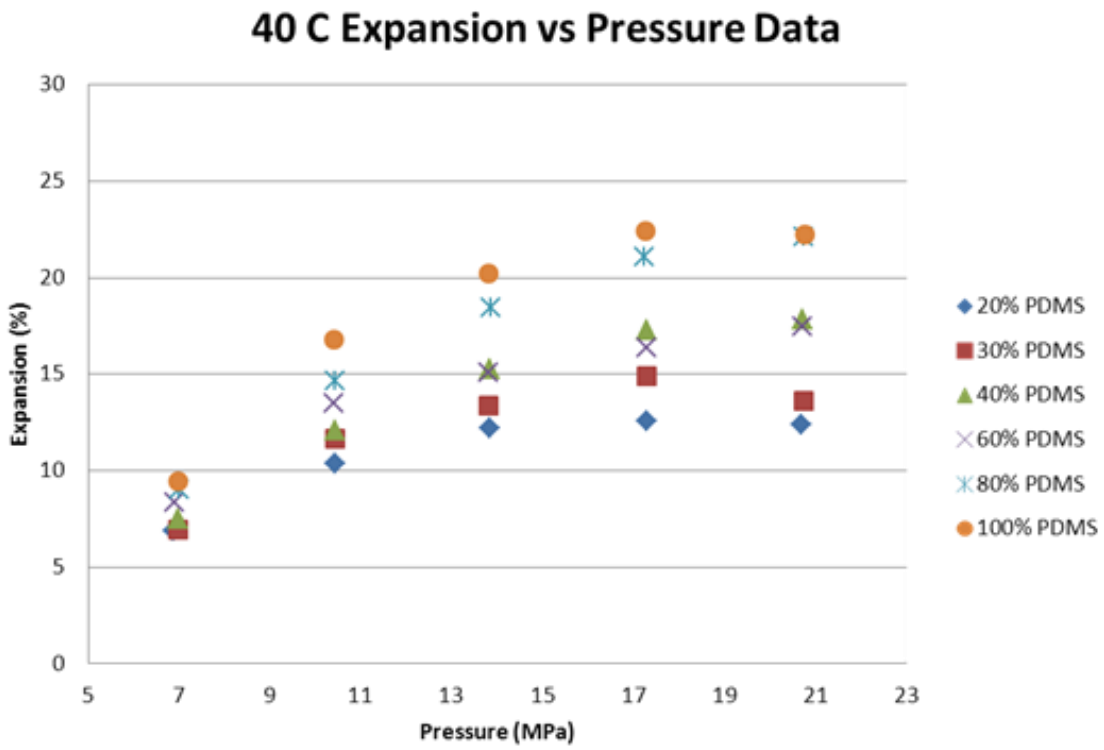

Figure 27: 40C Expansion Data as function of pressure for different concentrations of PDMS and copper particles

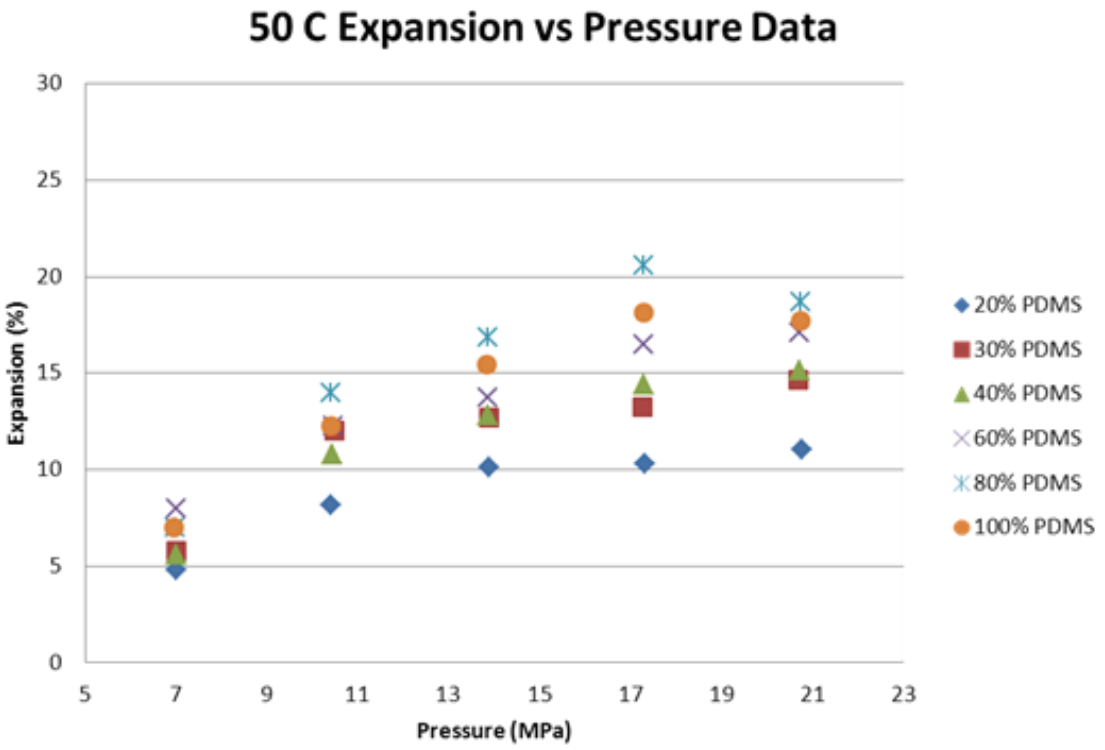

Figure 28: 50C Expansion Data as function of pressure for different concentrations of PDMS and copper particles

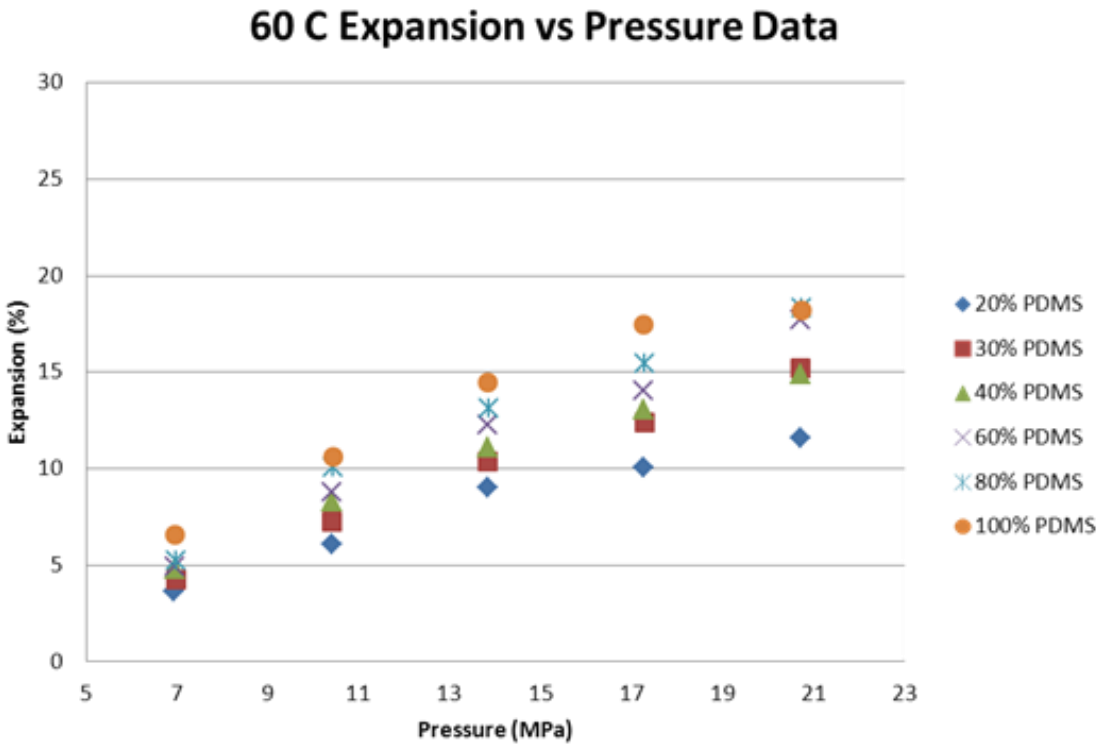

Figure 29: 60C Expansion Data as function of pressure for different concentrations of PDMS and copper particles

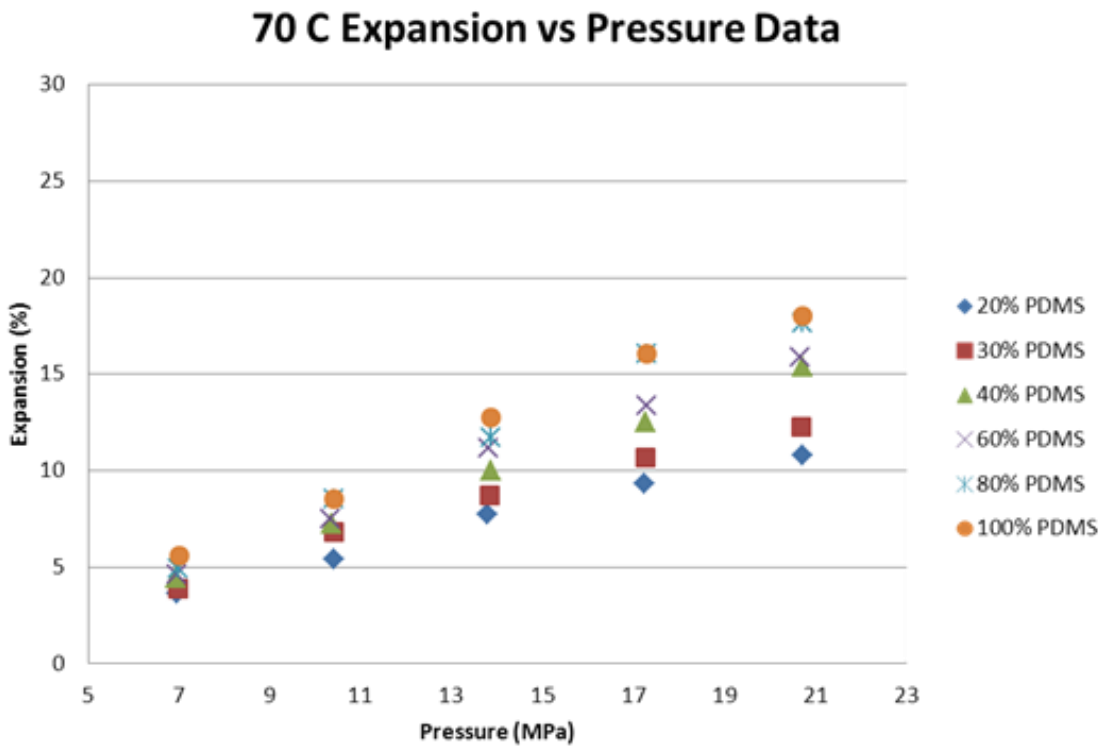

Figure 30: 70C Expansion Data as function of pressure for different concentrations of PDMS and copper particles

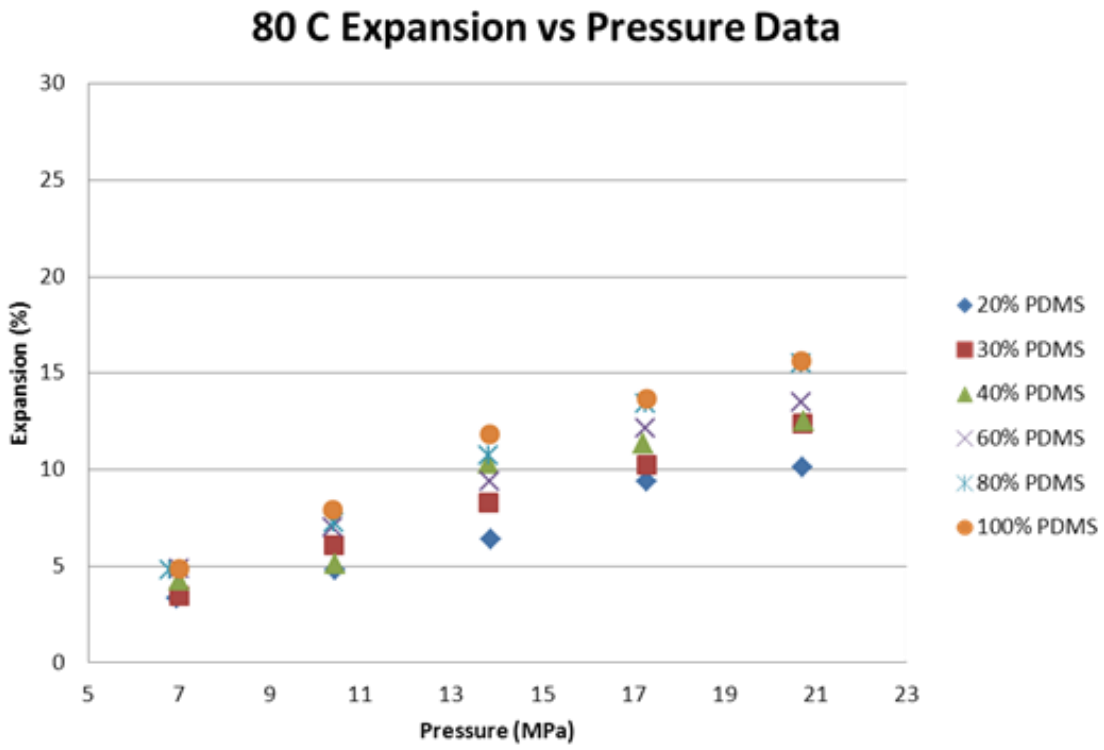

Figure 31: 80C Expansion Data as function of pressure for different concentrations of PDMS and copper particles

4.2. Expansion and PDMS Ratio

Expansion vs wt% data for all pressure and temperature is presented form Figure 32 to Figure 36. Ratio of PDMS and copper particle and expansion also formed a positive correlation. As expected the component of the sample that will expand is the primary factor in expansion. Higher ratio of PDMS results in more expansion was a reasonable trend. The positive linear correlation is evident. A more concise trend could be achieved if samples with 50 wt%, 70 wt%, and 90 wt% PDMS were experimented. Maximum expansion was observed to occur with 100wt% PDMS samples for almost all pressures and temperatures. There were three cases where samples subjected to 2500 Psi (17.24MPa) expanded more than samples subjected to 3000 Psi (20.68MPa). These data points occurred in the 40 C data and the 50 C data. Results from the 40 C and 50 C data sets seemed to be more erratic and unpredictable. The reason for this erratic

and unpredictable behavior could be that the pressure and temperature the experiment conducted under was close the high density fluctuation ridge for CO2. The trend formed by each pressure groups are well separated for each temperature sets.

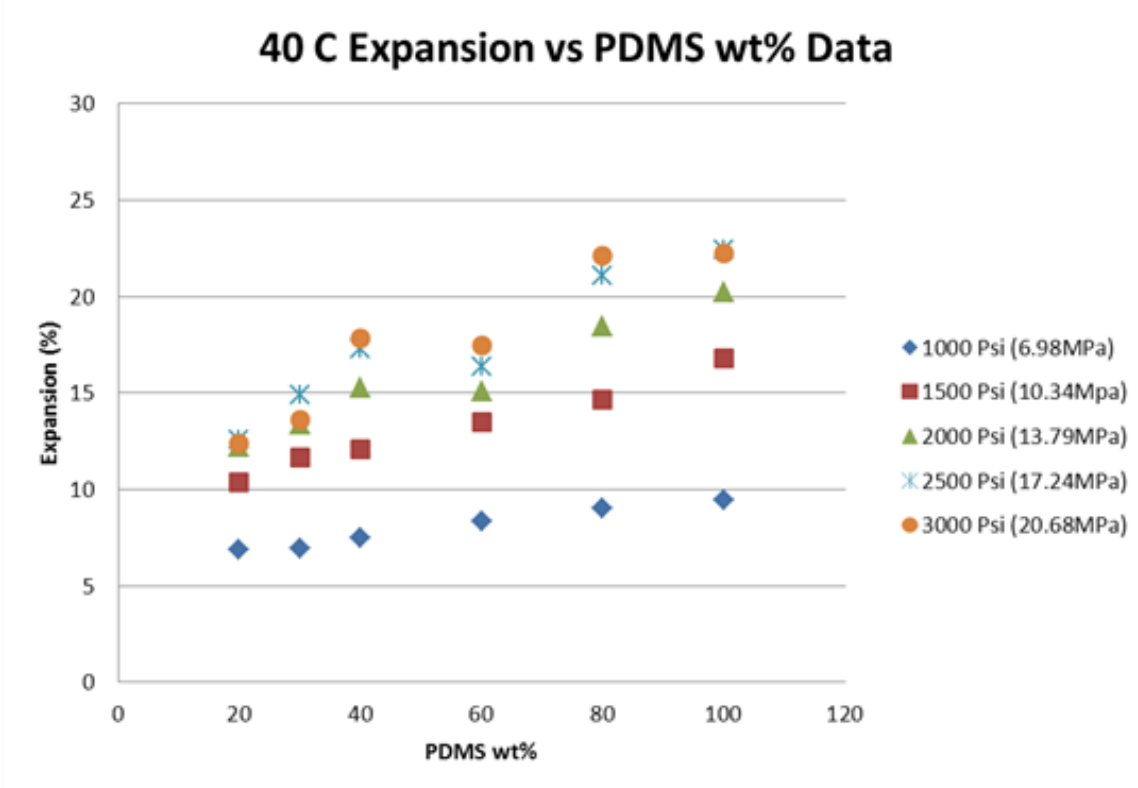

Figure 32: 40C Expansion Data as function of PDMS ratio for different pressures ranging from 1000 Psi (6.98MPa) to 3000 Psi (20.68)

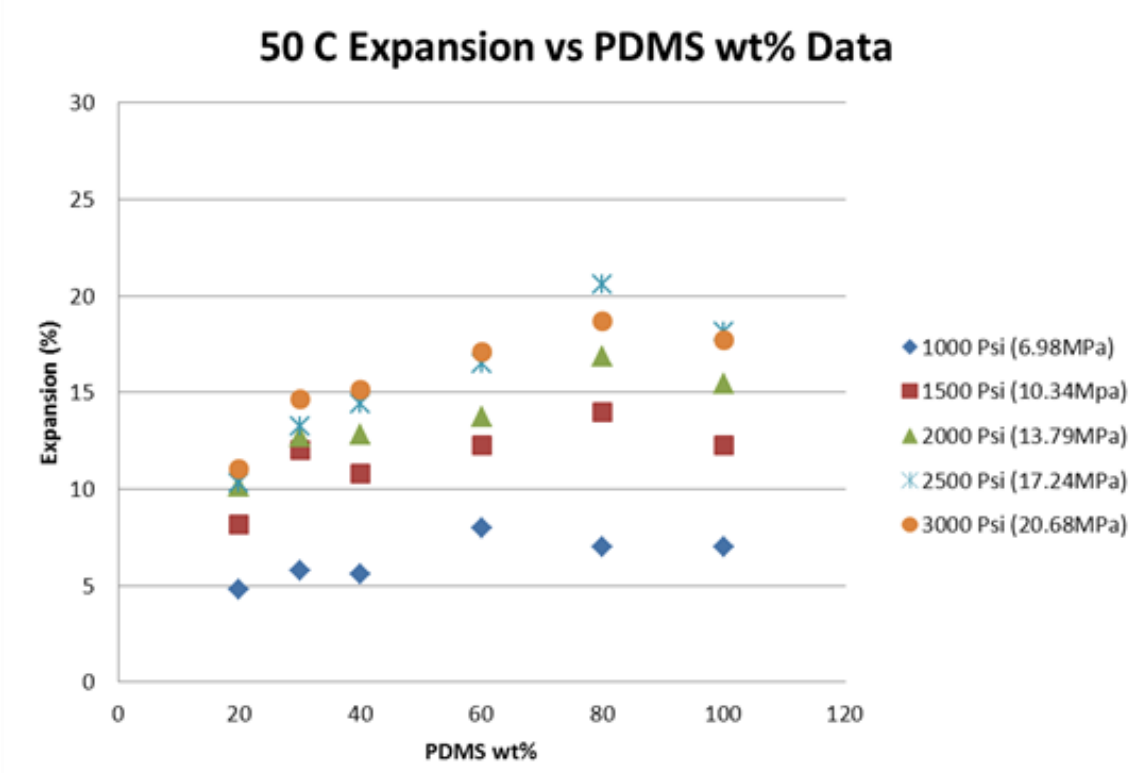

Figure 33: 50C Expansion Data as function of PDMS ratio for different pressures ranging from 1000 Psi (6.98MPa) to 3000 Psi (20.68)

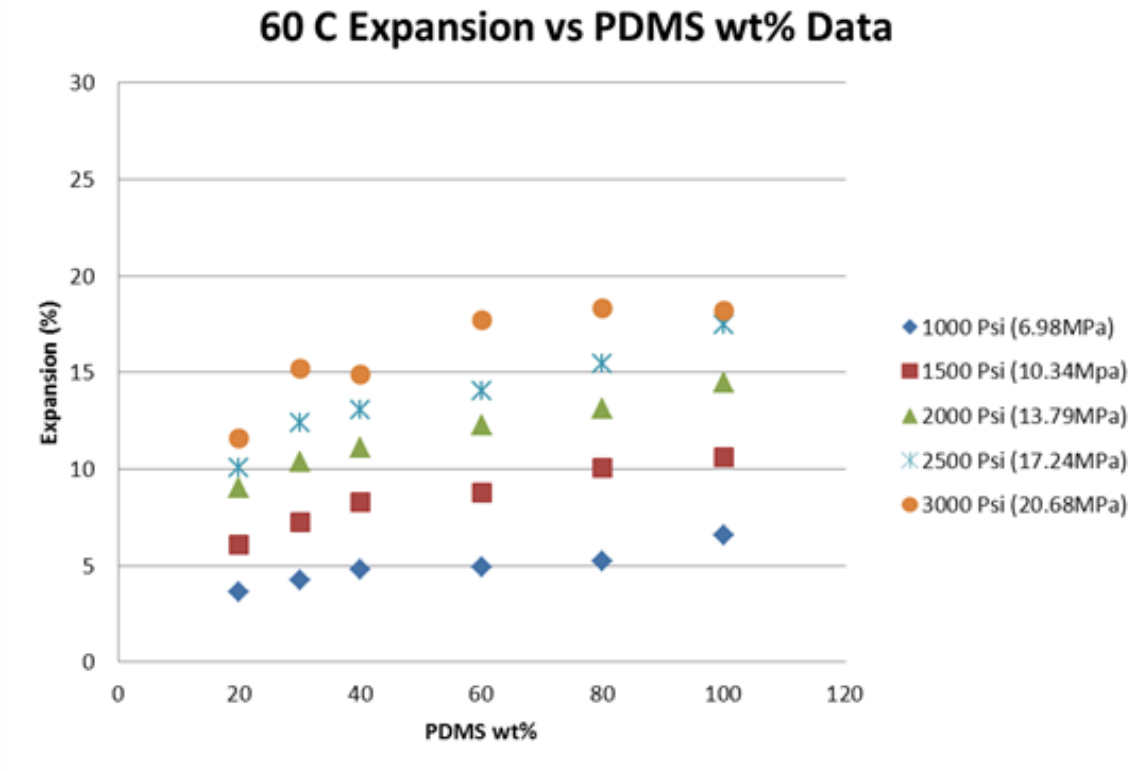

Figure 34: 60C Expansion Data as function of PDMS ratio for different pressures ranging from 1000 Psi (6.98MPa) to 3000 Psi (20.68)

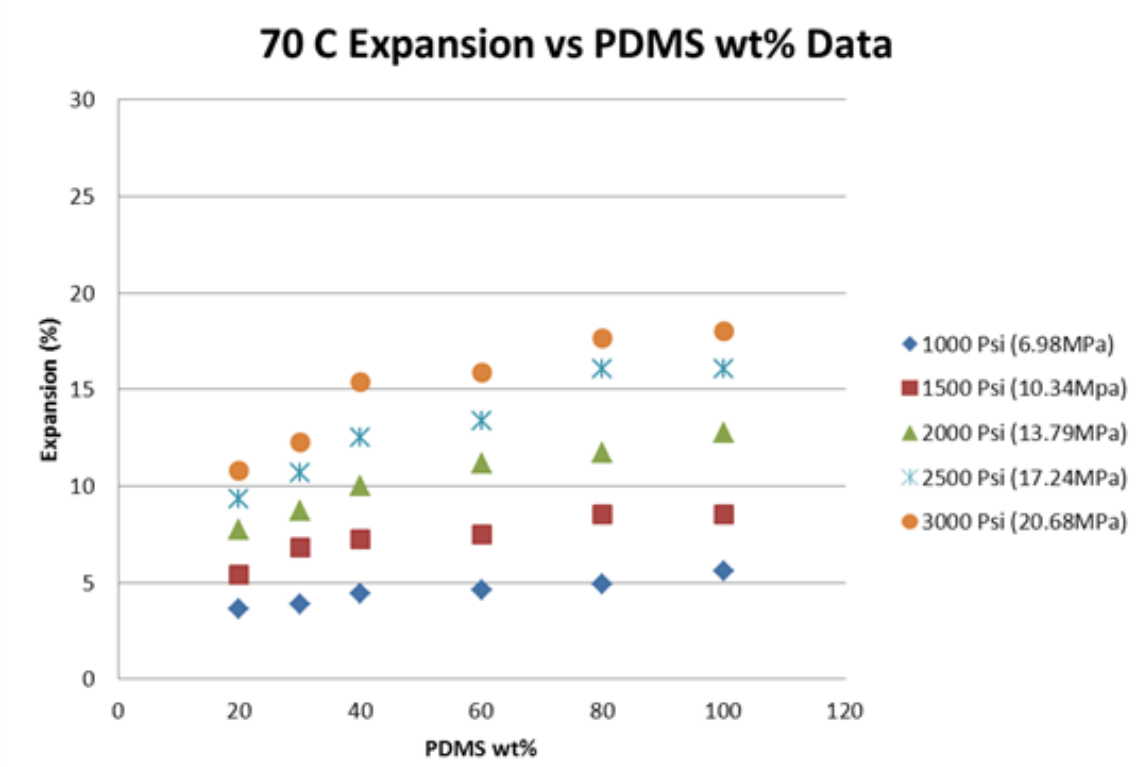

Figure 35: 70C Expansion Data as function of PDMS ratio for different pressures ranging from 1000 Psi (6.98MPa) to 3000 Psi (20.68)

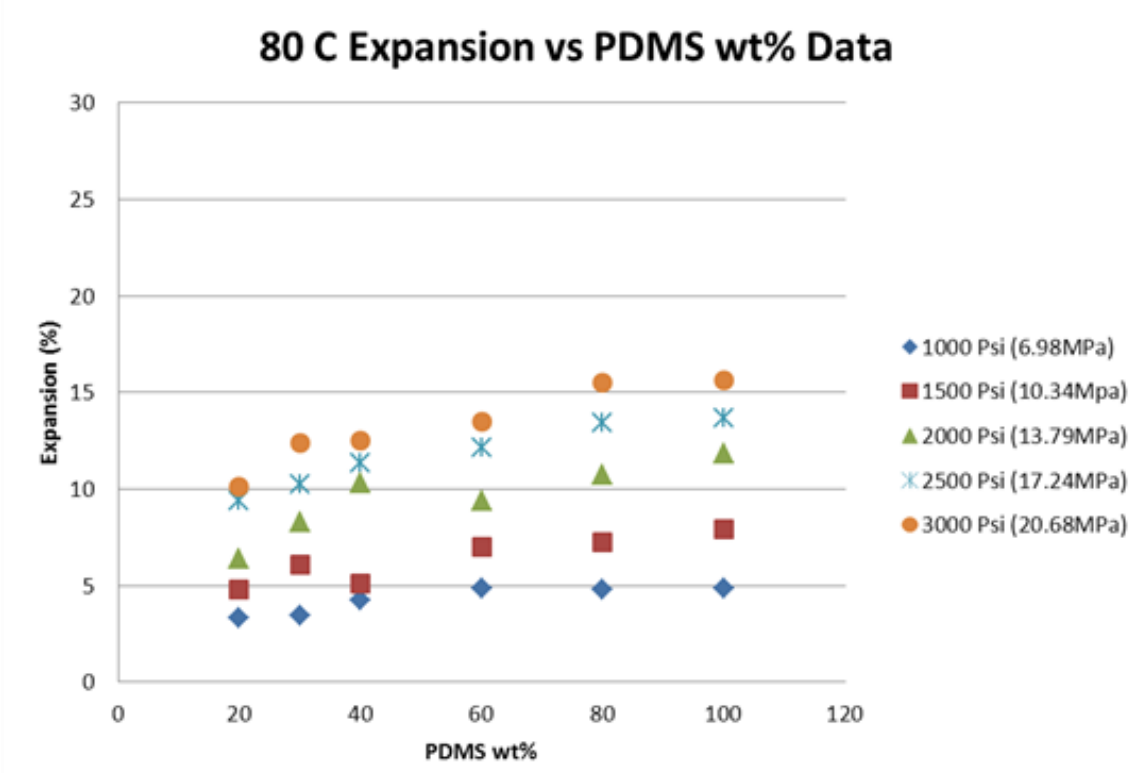

Figure 36: 80C Expansion Data as function of PDMS ratio for pressures ranging from 1000 Psi (6.98MPa) to 3000 Psi (20.68)

4.3. Expansion and Temperature

Expansion vs Temperature data for all pressure and PDMS ratio is presented form Figure 37 to Figure 41. As temperature increased, expansion decreased, this was not expected. This could be explained by Whitesides' theory. The difference of solubility parameter between PDMS and CO2 increases as temperature increases this will result in less expansion due to the incompatibility of the solvent and solute. The results from lower pressure are much more predictable than the results from higher pressure. This could be the result of density fluctuation of scCO2, or errors from the experimental setup.

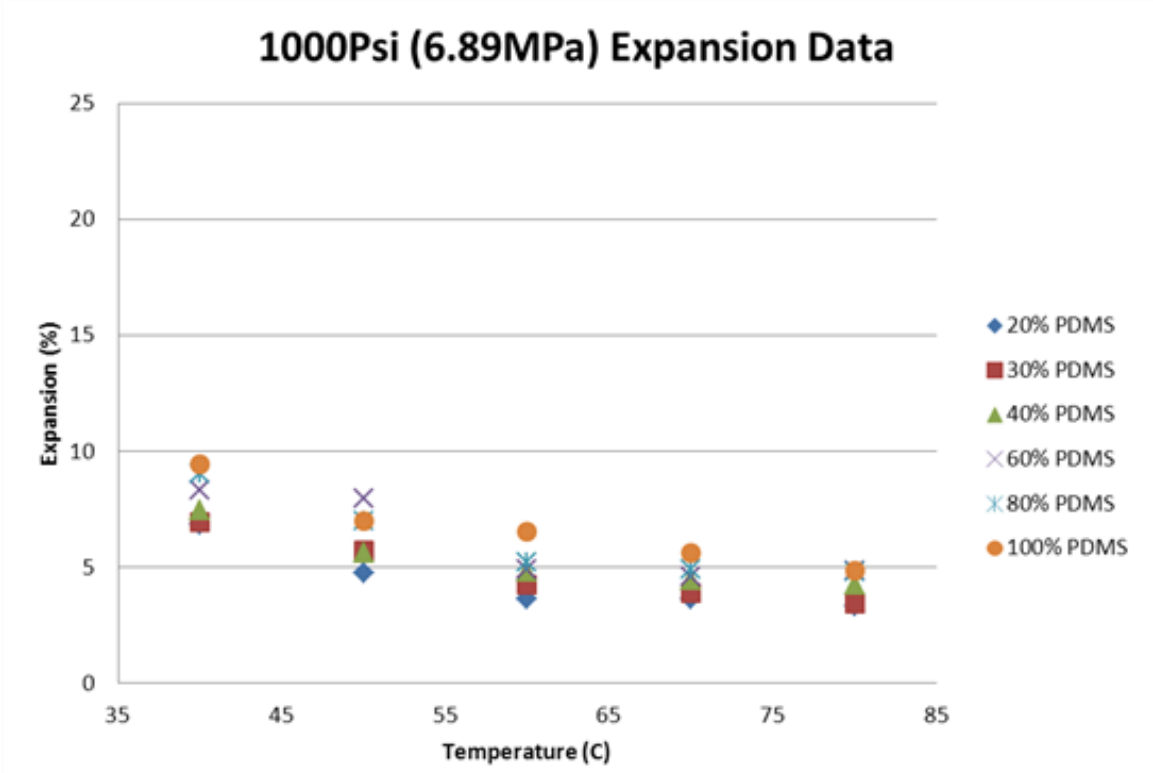

Figure 37: 1000Psi (6.89MPa) Expansions as a function of temperature for different PDMS sample concentrations

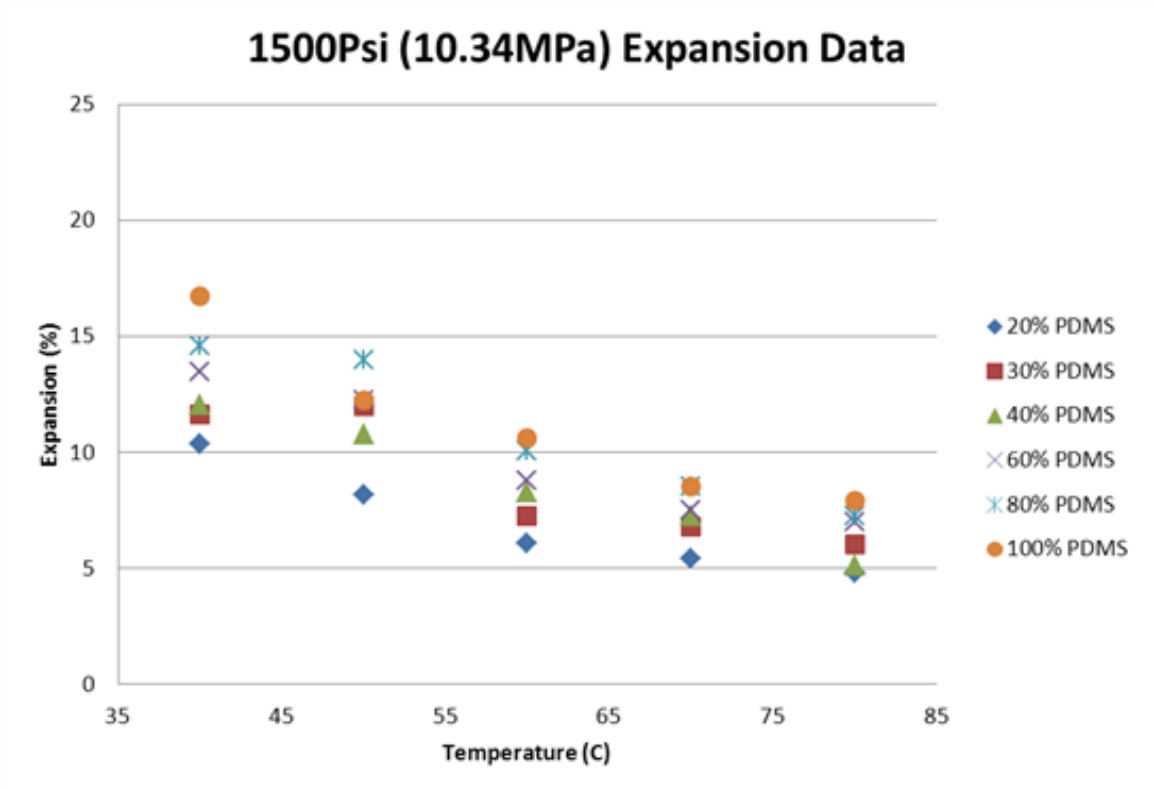

Figure 38: 1500Psi (10.34MPa) Expansions as a function of temperature for different PDMS sample concentrations

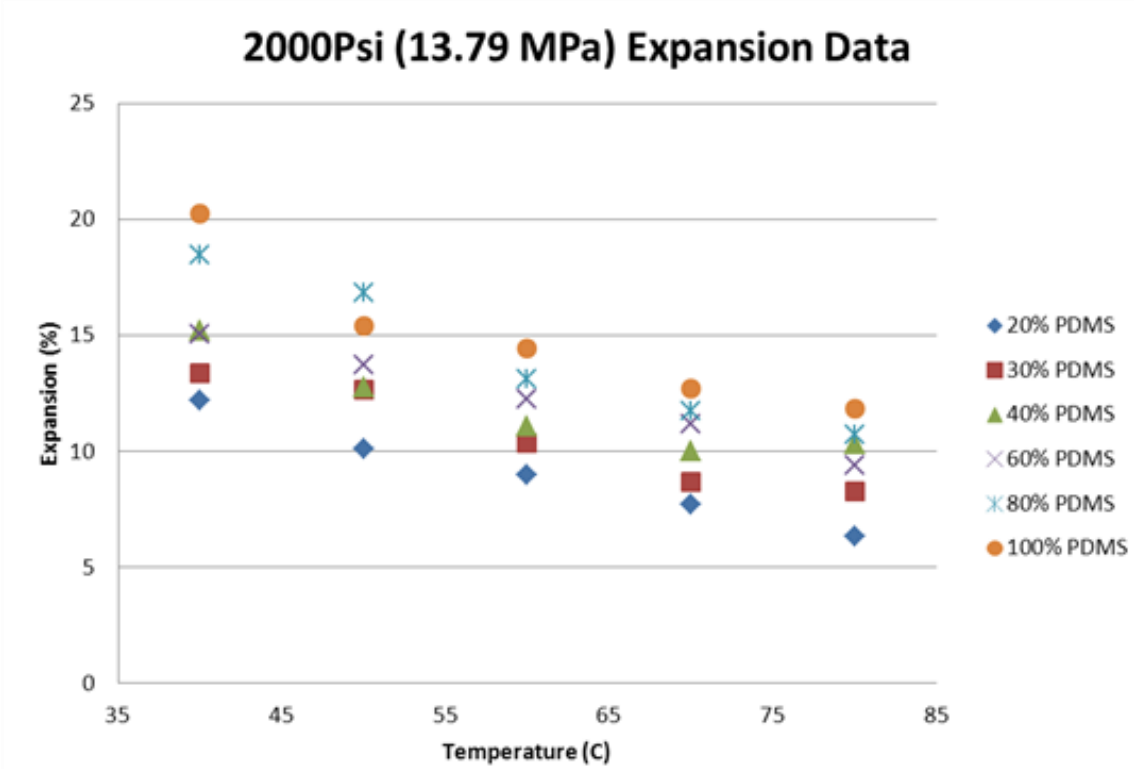

Figure 39: 2000Psi (13.79MPa) Expansions as a function of temperature for different PDMS sample concentrations

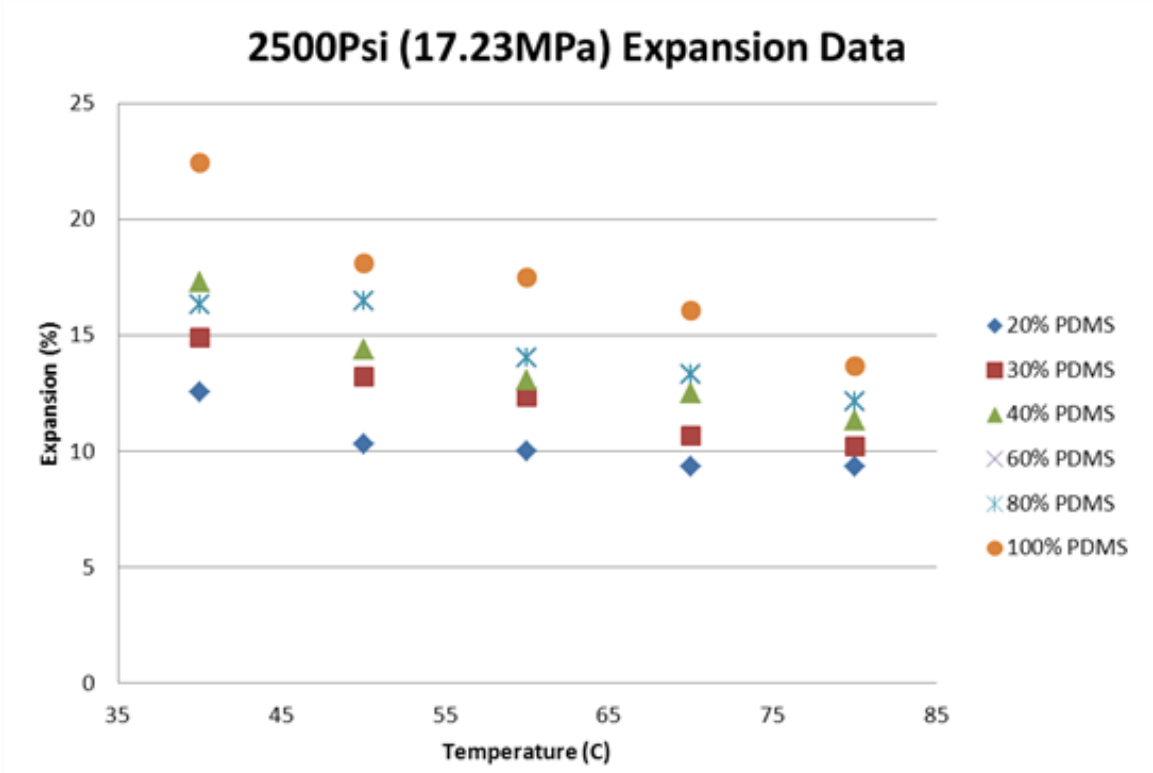

Figure 40: 2500Psi (17.23MPa) Expansions as a function of temperature for different PDMS sample concentrations

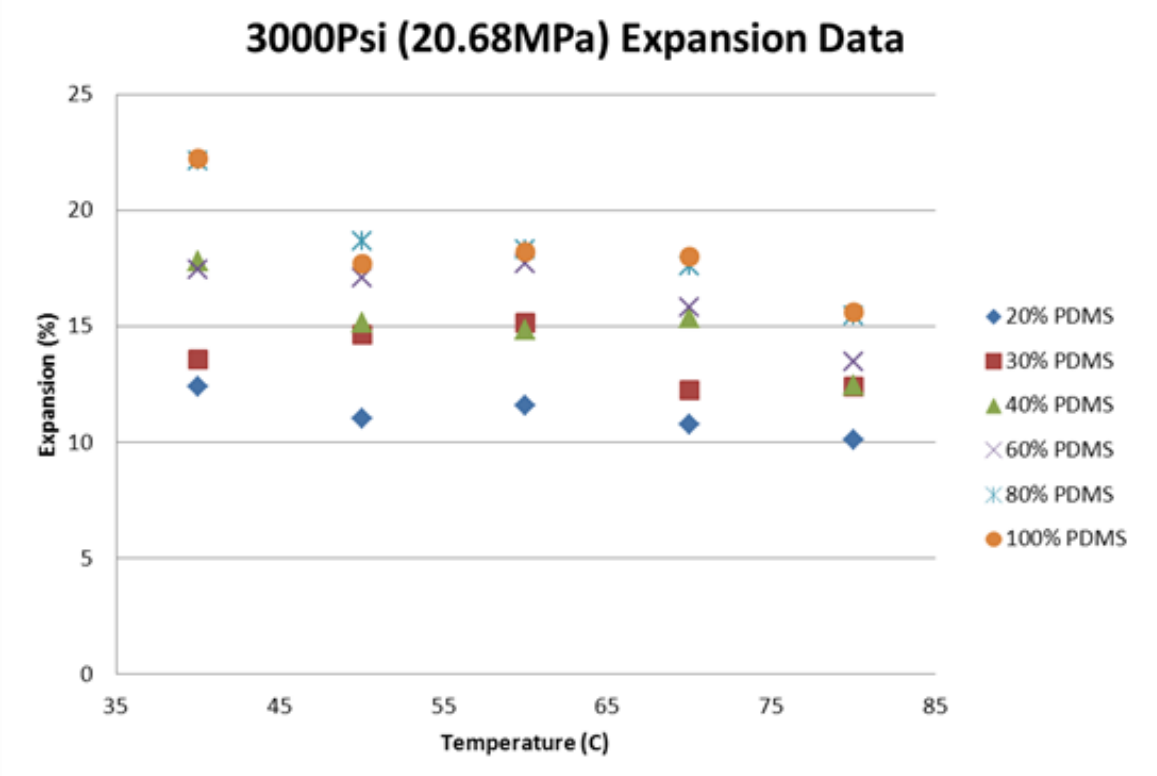

Figure 41: 3000Psi (20.68MPa) Expansions as a function of temperature for different PDMS sample concentrations

4.4. Time Constant and Pressure

Time constant vs Pressure data for all PDMS ratios and temperature is presented form Figure 42 to Figure 46. It took longer for the sample to reach equilibrium in lower temperature experiments. One of the reasons for this was that the lower temperature samples expanded more. It also took longer for the higher pressure to build up in the view cell. The syringe pump has a limit flow rate; therefore it will have a longer pressurization time if the targeted pressure is higher. It is generally the case for lower PDMS ratio samples to reach equilibrium faster than the higher PDMS ratio samples. This trend is much more obvious in the higher temperature data sets. The copper particles block the path of scCO2 diffusing into the sample so the scCO2 will have to travel much further to reach the PDMS at the center of the sample.

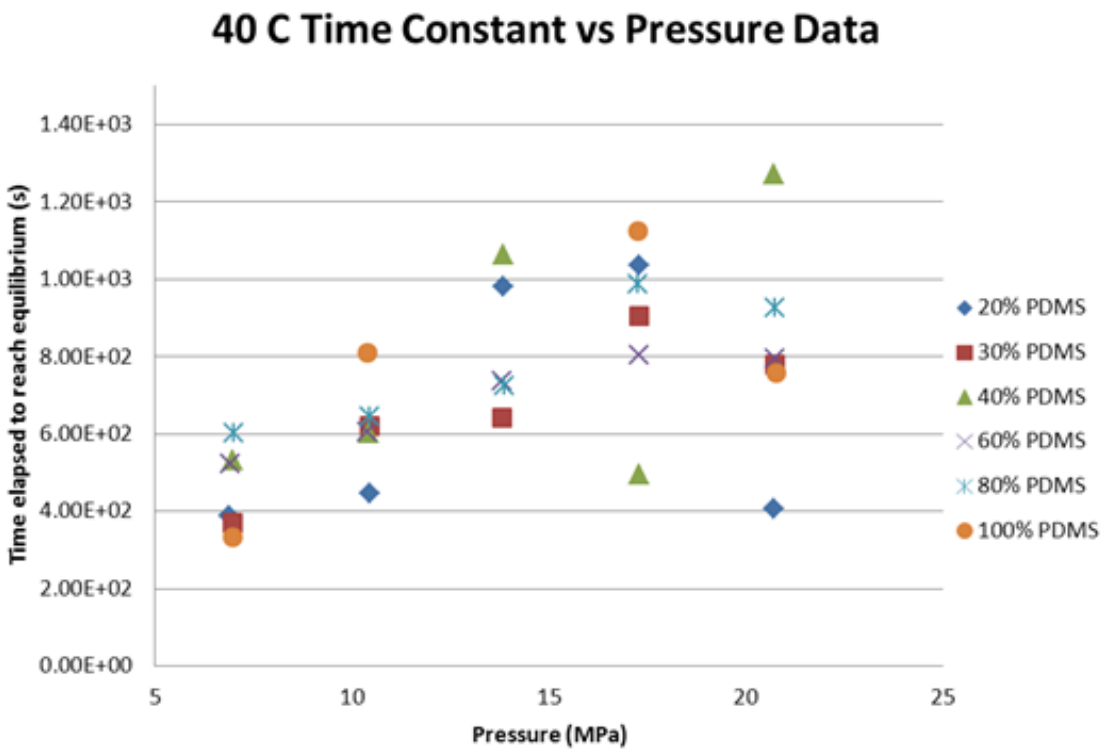

Figure 42: 40C Time constant data as a function of Pressure for all PDMS sample concentrations

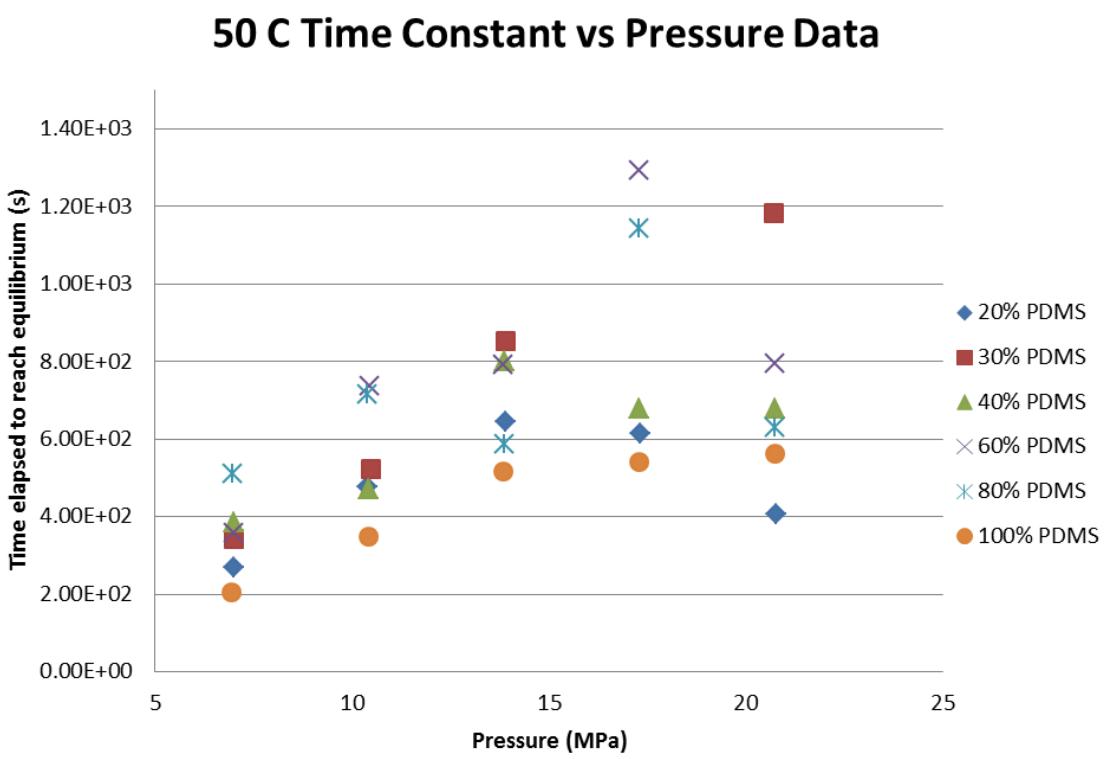

Figure 43: 50C Time constant data as a function of Pressure for all PDMS sample concentrations

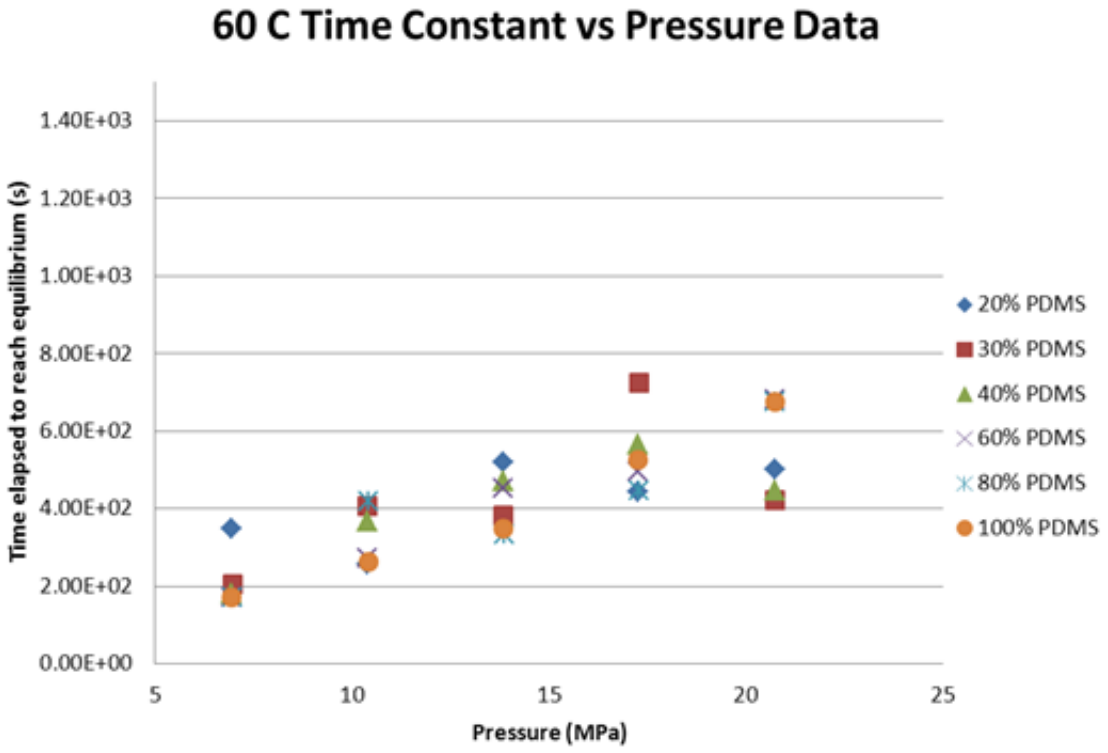

Figure 44: 60C Time constant data as a function of Pressure for all PDMS sample concentrations

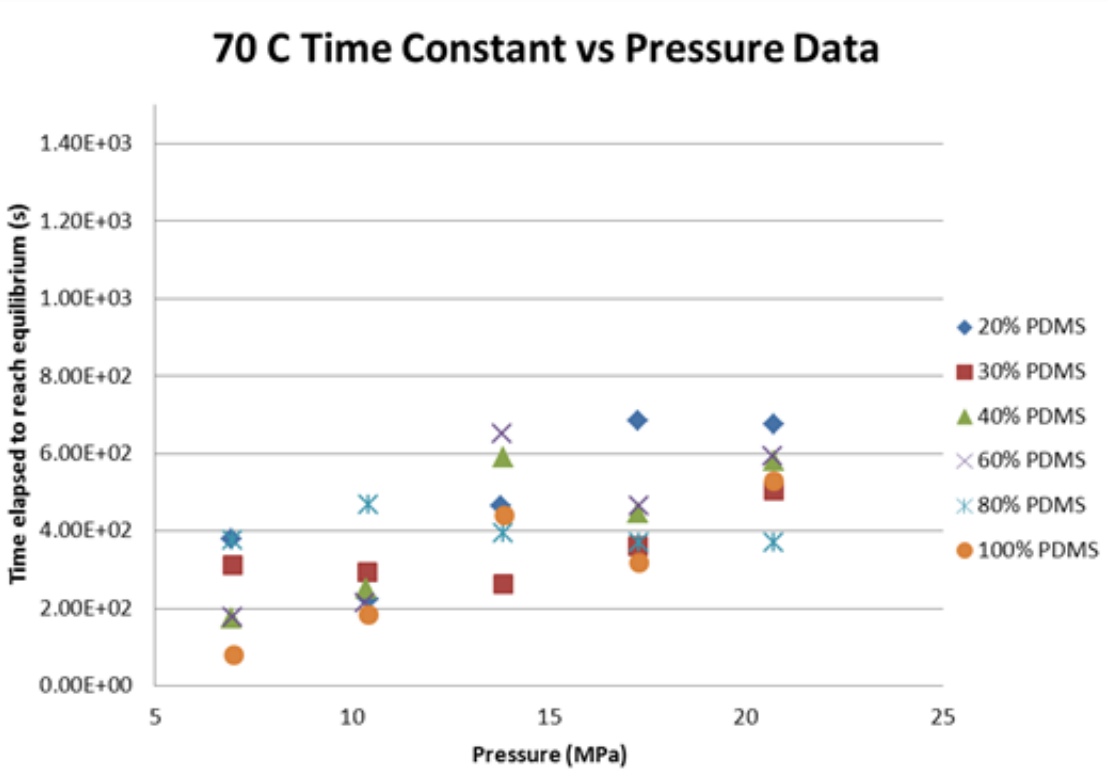

Figure 45: 70C Time constant data as a function of Pressure for all PDMS sample concentrations

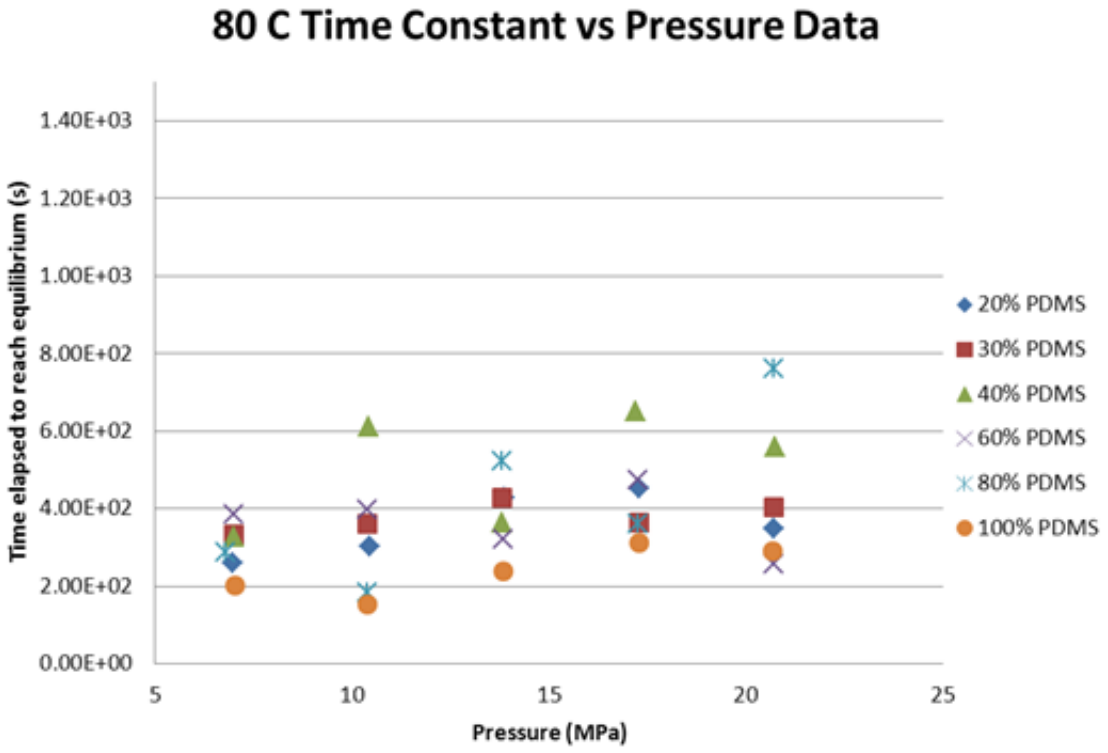

Figure 46: 80C Time constant data as a function of Pressure for all PDMS sample concentrations

4.5. Expansion and Time Constant

Expansion vs time constant data for all PDMS ratio and temperature is presented from Figure 47 to Figure 51. It was observed that greater overall expansion will take longer to reach the expansion equilibrium. This formed a positive relationship as seen in the scatter plotted results for all temperature ranges. The positive correlation becomes much weaker as temperature increase. At lower temperature both the time it took for the sample to reach equilibrium and maximum expansion was increased. There seem to be no correlation between different concentrations of PDMS.

The time to reach equilibrium range from around 100 seconds (1.7 minutes) to around 1300 seconds (21.7 minutes). Time constant is mainly dependent on the amount of expansion experienced by the sample.

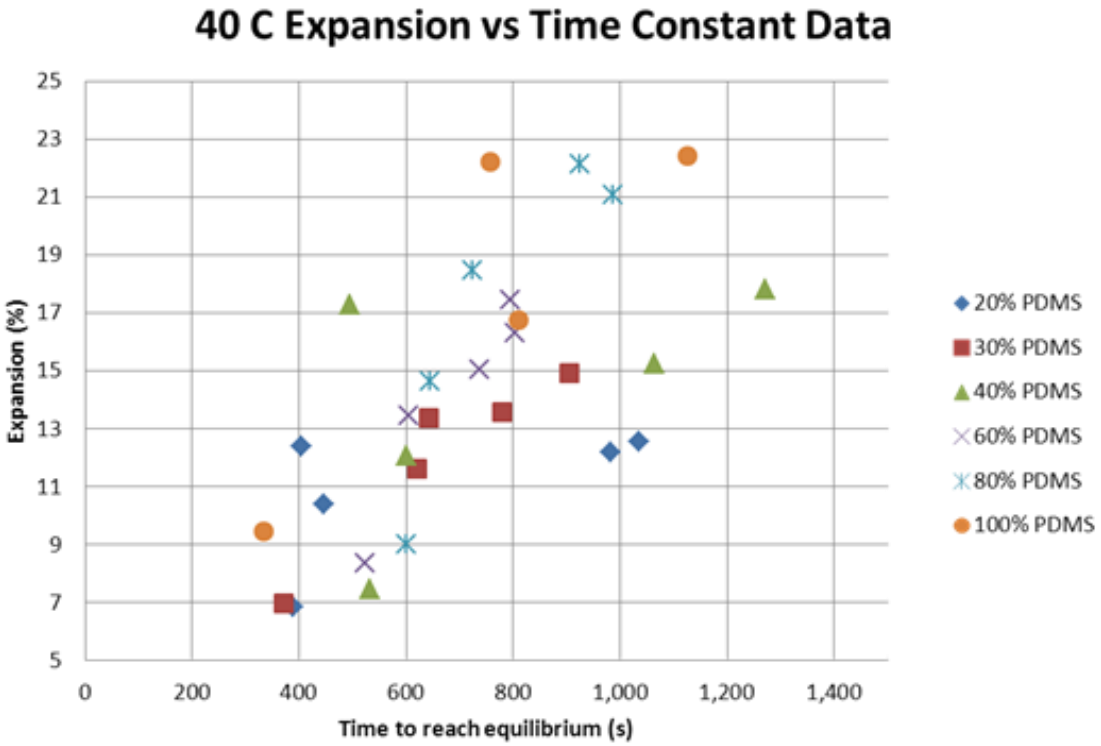

Figure 47: 40C Expansion as a function of time for different PDMS sample concentrations

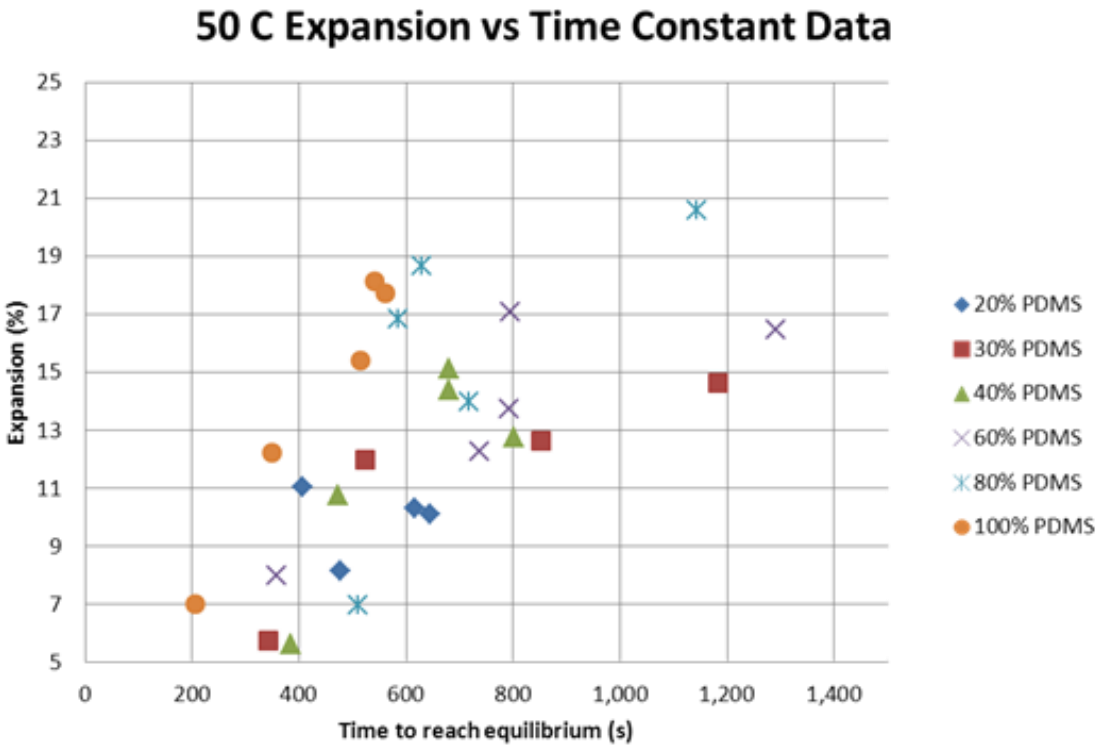

Figure 48: 50C Expansion as a function of time for different PDMS sample concentrations

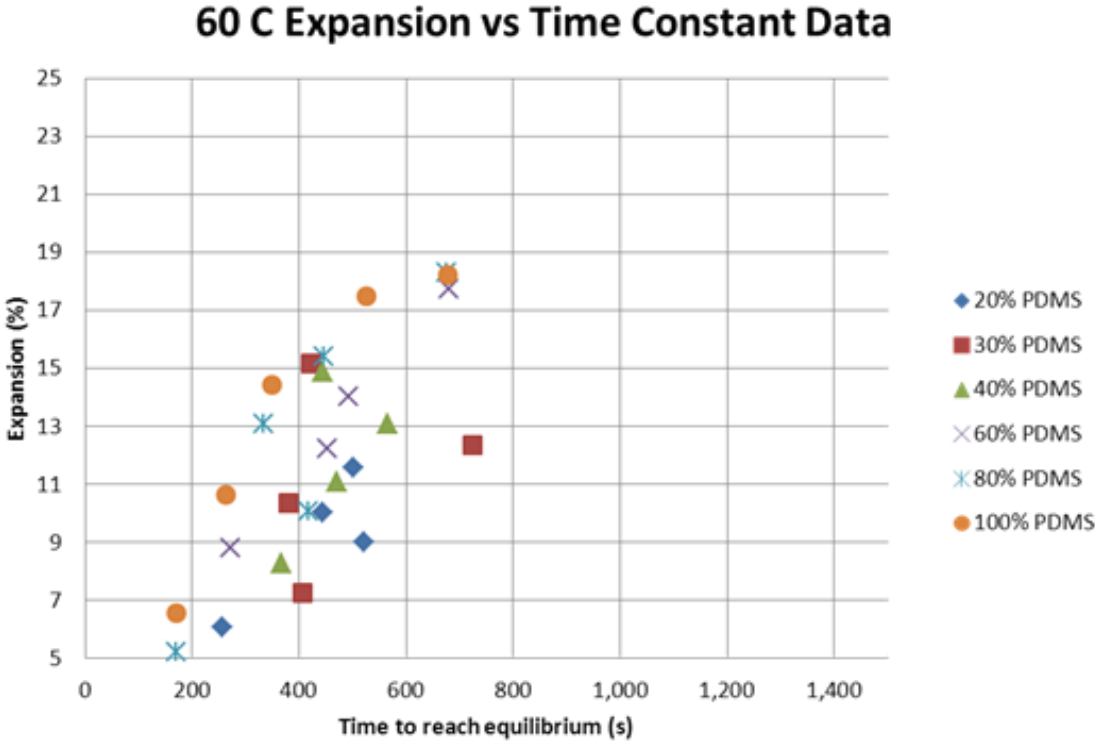

Figure 49: 60C Expansion as a function of time for different PDMS sample concentrations

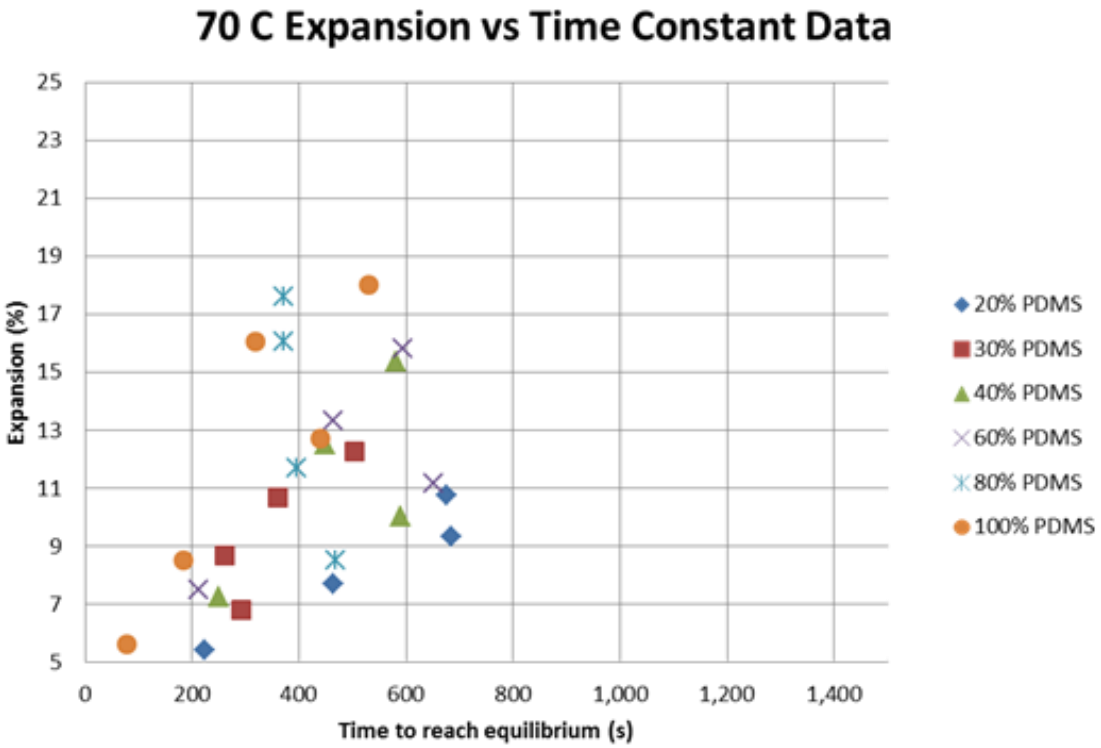

Figure 50: 70C Expansion as a function of time for different PDMS sample concentrations

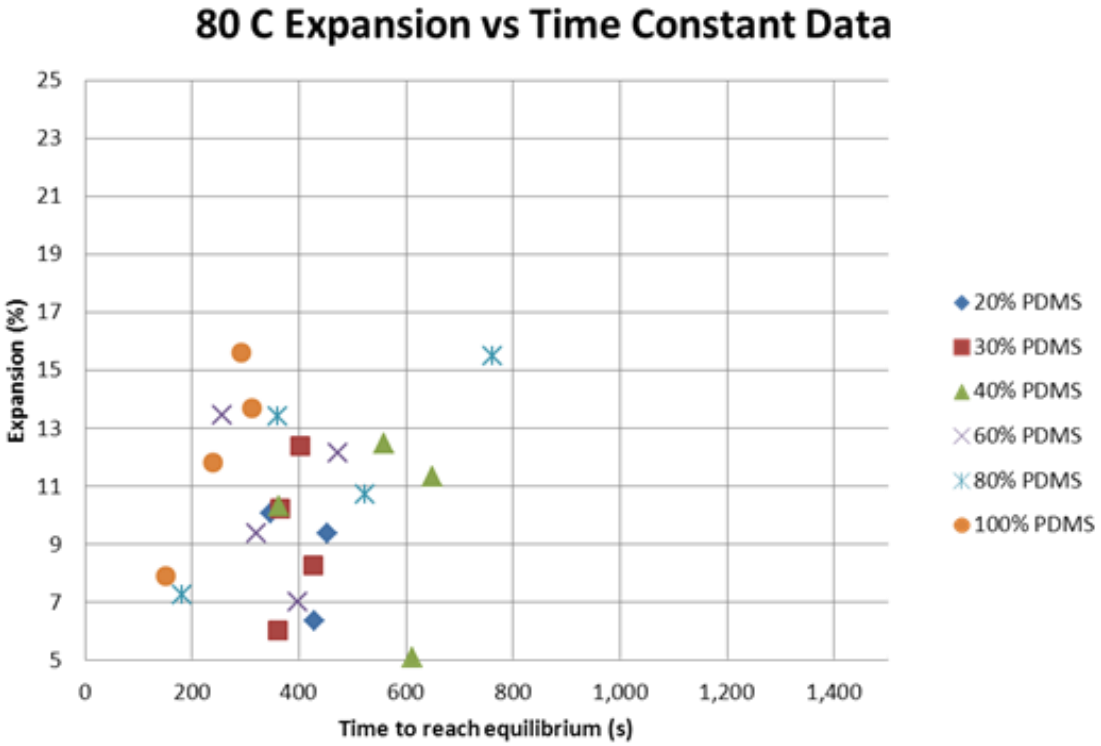

Figure 51: 80C Expansion as a function of time for different PDMS sample concentrations

4.5. Possible Errors

There are several sources for error in this investigation even though great care was taken to ensure experimental consistency. These errors will be discussed in this section.

4.5.1. Human Errors

The techniques and procedure might not be exactly the same form experiment to experiment due to few reasons. First reason is that all of the experiments were done by two individuals. This will result in slight differences in the procedural. Much of the experimental setup was automated and controlled by electronic controls but there are still part that was controlled by humans. For example: the valves on the view cell apparatus were controlled by humans, so there are going to be slight differences in how fast it opens and closes every time. This was the primary reason that the decompression data was not available because there was no consistent way of opening the valves; this also has influence the time it took to reach equilibrium for samples.

4.5.2. Equipment Errors

There are a few errors that could be avoided by perfecting experimental design and experimental setup construction. The CO2 concentration fluctuation discussed in the introduction can be avoided if temperature and pressure is chosen differently. This could have changed the result slightly. The thermocouple was placed with in the thickness of the view cell wall. The reason for this placement was that if the thermal couple protrudes into the test chamber any more it would be prohibiting the sample holder from being placed inside the view cell. The negative of this set up is that the thermocouple could not read the temperature at the

center of view cell (where the sample was). The reading from the thermocouple was going to be closer to the temperature of the view cell wall. Some of the resulting expansion curves might be the result of the near 0 C CO2 that did not have a chance to warm up to the set temperature. Figure 52 presents an expansion curve that exhibit irregular data points that could been caused by initial temperature differences. Errors like this could be minimized if the experiments can be repeated and the results are the average of the different repetitions. Errors could have compounded in the experiments carried out for this investigation. The errors made in the production of the PDMS sample added to the errors made in the view cell experiment will result in the errors in the expansion curve and by the time the expansion is curve fitted the error could be very significant.

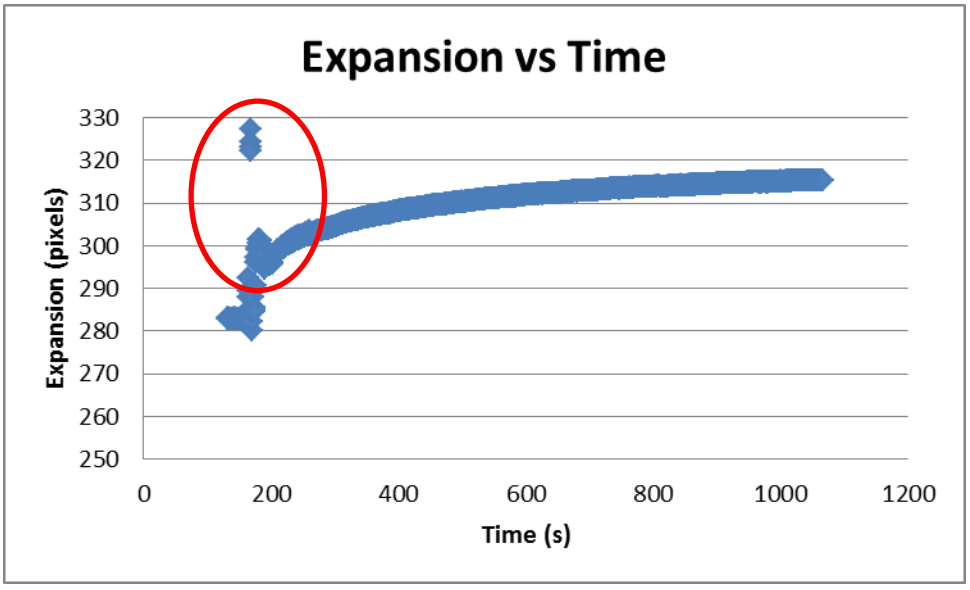

Figure 52: expansion curve with irregular data points during pressurization

Chapter 5. Conclusion

The expansion and the time constant data of PDMS and copper particle composite in this investigation have not been published previously. Basic expansion characteristic of PDMS-copper particle composite in CO2 was defined. This will provide a starting point for improved fabrication process for MEMS metal-polymer composite sensor element. The data gathered in this study can be used to target specific expansion of a PDMS-copper particle composite by adjusting pressure and temperature of CO2.

PDMS-copper particle composite expansion is positively correlated to CO2 pressure. Most expansion observed for all temperature and PDMS to particle ratio occurred at higher pressure, 2500Psi (17.24Mpa) and 3000Psi (20.68MPa). The least expansion occurred at lowest pressure, 1000 Psi (6.98MPa). Temperature is negatively correlated to PDMS-copper particle composite expansion. As temperature increased expansion decreased, at 80 C, the highest temperature, the least expansion was observed. The most expansion occurred at the lowest temperature, 40 C. Negative correlation between expansion and temperature can be explained by Whitesides' theory. As temperature increase the difference between the solubility parameters becomes greater resulting in less compatibly between PDMS and CO2.

PDMS to copper particle ratio is positively correlated to expansion. As the PDMS portion of the sample increases the overall expansion of the composite increases. This result was within expectations. Copper should not have any volumetric changes when submersed in CO2 so the driving factor of the composite expansion is the PDMS portion of the composite. Pure PDMS generally experienced the most expansion for all temperature and pressure data sets. Samples with 80 wt% copper (20 wt% PDMS) experienced the least expansion for all temperature and pressure data sets. Copper particles are inhibitors for expansion of the combined composite.

Time constant and expansion observed is positively correlated. it generally took longer to reach greater expansion. This could be the results of two factors. First factor is that it took longer for the test camber to reach the higher pressure where greater expansion was observed. Second factor is the increased shear energy involved as the sample expands.

The expansion data have shown expansion of PDMS-copper composite can be achieved. The expansion of 20% PDMS samples is vary from around 2% to 12%. This means that in-situ etching of oxide using scCO2 expansion technique with PDMS imbedded with copper particles can be attempted. Furthermore the basic parameters for PDMS expansion with scCO2 technique are now known.

The data from this thesis work is compared with data form Eckert's group and can be seen in Figure 53 [12] where both sets of data is over-laid on top of each other with the same scale. The pressure range studied by Briscoe was from 0 bar to 200 bar whereas this thesis work studied pressure ranging from 69.8 bar (6.98 MPa) to 206.8 bar (20.68 MPa). The difference between the data could be attributed to the difference in the PDMS source, the curing process, geometry of the sample, and the pressurization method. The literature by Eckert stated a different vendor for the PDMS, and PDMS films were used in the experiments. The method for PDMS curing was not discussed.

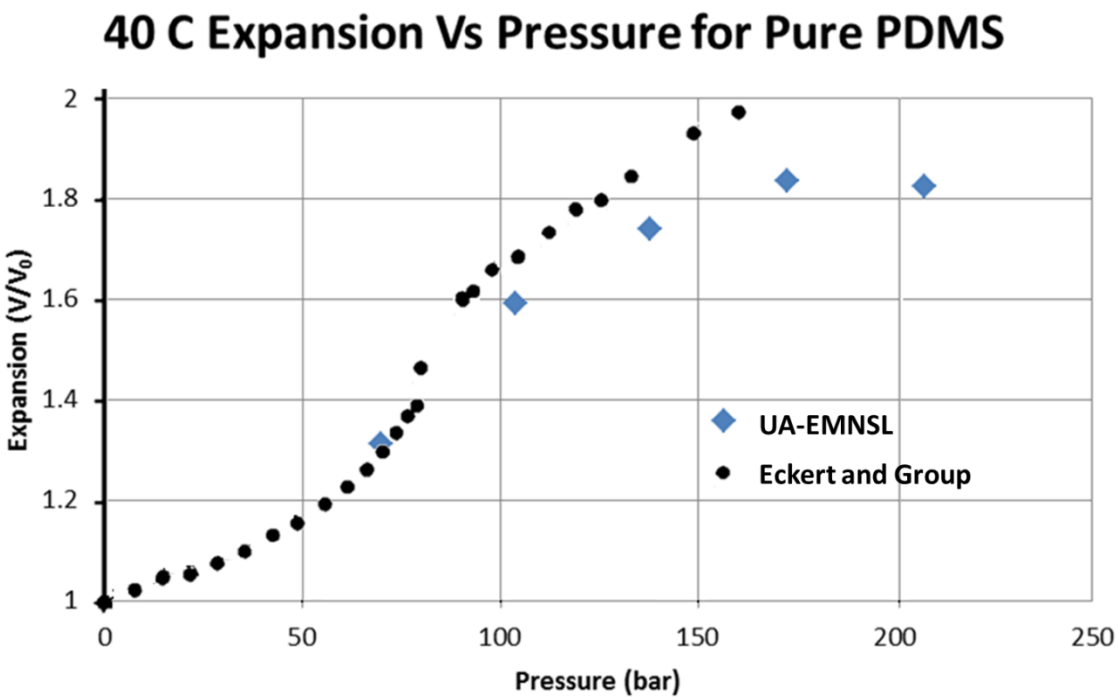

Figure 53: 40 C expansion data form Ekert and group compared to 50 C expansion data from this investigation. The data is over-laied to the same scale [12].

Chapter 6. Future Work

Next step is to develop the parameters needed to mix CO2 and etching agent. In order to accomplish this step, a new experimental set up is needed, an appropriate etching agent have to be chosen, and PDMS-metal composite sensing element samples have to be made.

The new experimental setup requires a new syringe pump, a system that will allow mixing of the scCO2 and an etching agent. In addition to replicating the conditions of this thesis work, the new system has to cool down to at least 20 C to allow greater expansion or to reduce the pressure requirement. Multiple factors have to be considered for the etching agent, the inertness, etching strength, availability, and chemical compatibility. Extensive literature search is need to find the optimal etching agent. The sensing element sample can be made through the DEPPOST fabrication process. Sensor sized, the metallic lead gap, and wafer arrangement have to be considered.

Works Cited

[1] F. Pan, "Preliminary Development of MEMS-Based Corrosion Senso, Thesis," University of Arkansas, Fayetteville, AR, 2010.

[2] T. Tanaka and D. J. Fillmore, "Kinetics of swelling of gels," J. Chem. Phys., pp. 1214-1218, 1 Feb 1979.

[3] J. N. Lee, C. Park and G. M. Whitesides, "Solvent Compatibility of Poly(dimethyliloxane) bassed microfluidid deices," Analytical Chemistry, pp. 6544-6554, 2003.

[4] A. Goodman, "A Comparison Study of Carbon Dioxid Adsorption on Polydimethyliloxane, silica Gel and Illinois No. 6 Coal Using in Situ Infarared Spectoscopy," Energy & Fuels, pp. 1101-1106, 2009.

[5] V. S. Agarwala and S. Ahmad, "Corrosion Detection and Monitoring - A Review," Corrosion2000, pp. 00271.1-00271.19, 2000.

[6] A. Huang, "Design and Fabricaton of the Nano-Particle Composite MEMS Corrosion Sensor," in 2008 ADME International Mechanical Engineering Congress and Exposition, Boston, MA, 2008.

[7] A. Huang, V. T. S. Wong and C.-M. Ho, "Silicone polymer chemical vapor sensor fabricated by direct polymer patterning on substarte techneque," Sensors and Actuators , vol. B, no. 116, pp. 2-10, 2006.

[8] G. V. Casquillas, "PDMS : A review," 2 April 2012. [Online]. Available: http://elveflow.com/microfluidic/69-pdms-and-microfluidic. [Accessed 2 April 2012].

[9] J. C. Lotters, W. Olthuis, P. H. Veltink and B. P, "The Mechanical Properties of Rubber Elastic Polymer Polydimethysiloxane for sensor applications," J. Micromech. Microeng, pp. 145-147, 1997.

[10] J. C. Mcdonald, D. C. Duffy, J. R. Anderson, D. T. Chlu, H. Wu, O. J. Schueller and G. M. Witesides, "Fabrication of Microfluidic Systems in Poly(dimethylsiloxane),"

Elecrophoresis, pp. 27-40, 2000.

[11] M. Roth, "Solubility Parameter of Poly(dimethylSiloxane) as a function fo Temperature and chain length," J. Polym. Sci.: PHys. ED, pp. 2715-2719, 1990.

[12] N. H. Brantley, D. Bush, S. G. Kazarian and C. Eckert, "Sectroscopic Measurement of Solute and Cosolvent Partitioning between Supercritical CO2 and Polymers," J. Phys. Chem. B, pp. 10007-10016, 1999.

[13] J. Y. K. C.-J. Kim, "Comparative Study of Variouse Release Methods for Polysilicon Sruface Micromachining," Proceedings, IEEE, pp. 442-447, 1997.

[14] T. Koga, Y. Seo and K. Shin, "The Role of Elasticity in Anomalous Swelling of Polymer Thin Film in Density Fluctuating Supercritical Fluids," Macromolecules, pp. 5236-5243, 2003.

[15] C. M. Hansen, Hansen Solublitiy Parameters a User's Handbook, Coca Raton, FL: Taylor and Francis Group, 2007.

[16] L. H. a. G. B. T.Tanaka, "Spectrum of Light Scatered From a Viscoelastic Gel," J. Chem. Phys., pp. 5151-5159, 1973.

[17] Y. Li and T. Tanaka, "Kinetics of Swelling and Shrinking of Gels," j. Chem. Phys., pp. 1365-1371, 1990.

[18] U.S. Secretary of Comerce, "Carbon Dioxide," 2011. [Online]. Available: http://webbook.nist.gov/cgi/cbook.cgi?ID=C124389&Units=SI&Mask=4#Thermo-Phase. [Accessed 9 April 2012].

[19] C. F. Beaton and G. F. Hewitt, physical property data for the design engineer, New York, Washington, Philadelpia, Londo: Hemispher publishing corporation , 1989 .

[20] "Thermocouples (TCs)," 1996-2008. [Online]. Available: http://www.temperatures.com/tcs.html. [Accessed 6 April 2012].

N. Flichy, S. Kazarian, C. Lawrence and B. Briscoe, "An ATR-IR Study fo
21] Poly(Dimethylsiloxane) under High-Pressure Carbond Dioxide: Simultaneouse Measurement of Sorption and Swelling," *J. Phys. Chem.*, vol. B, no. 106, pp. 754-759, 2002.

M. G. Fontana, Corrosion Engineering, New York: Tata McGraw-Hill Publishing
22] Company, 2005.

APPENDEX A

LabVeiw VI for DATA acquisition Front Panel

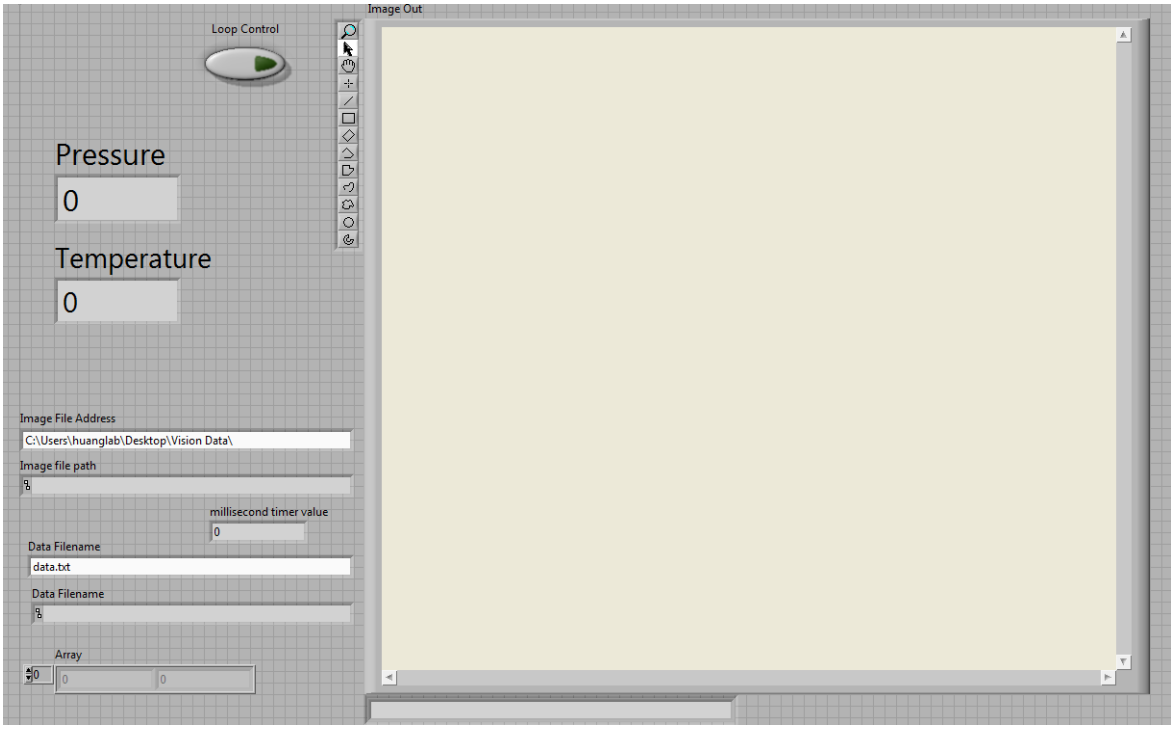

LabVeiw VI for DATA acquisition Block Diagram

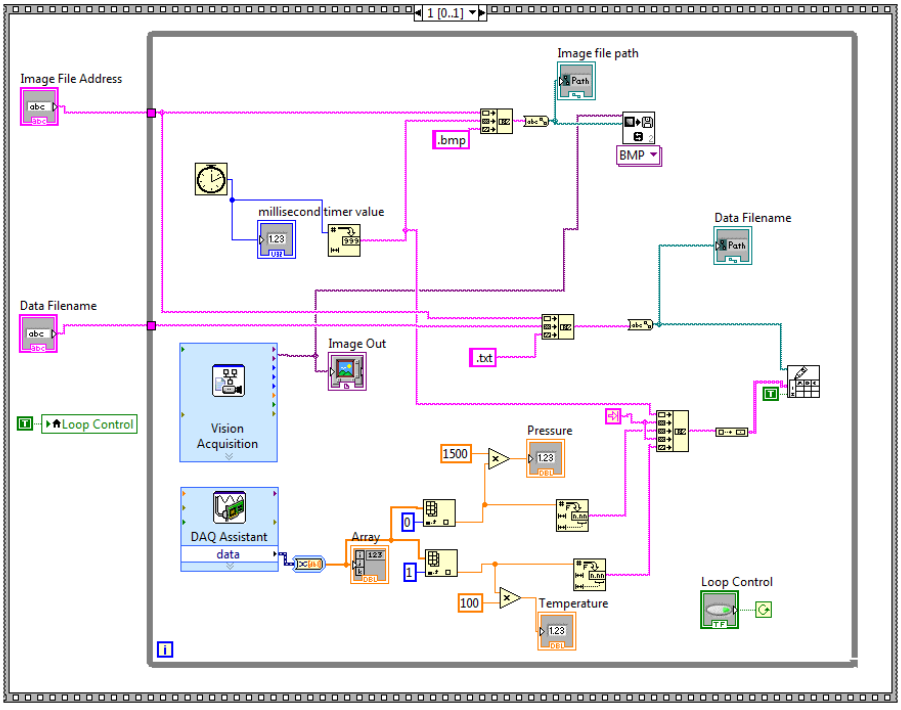

APPENDEX B

LabVeiw VI for Edge detection Front Panel

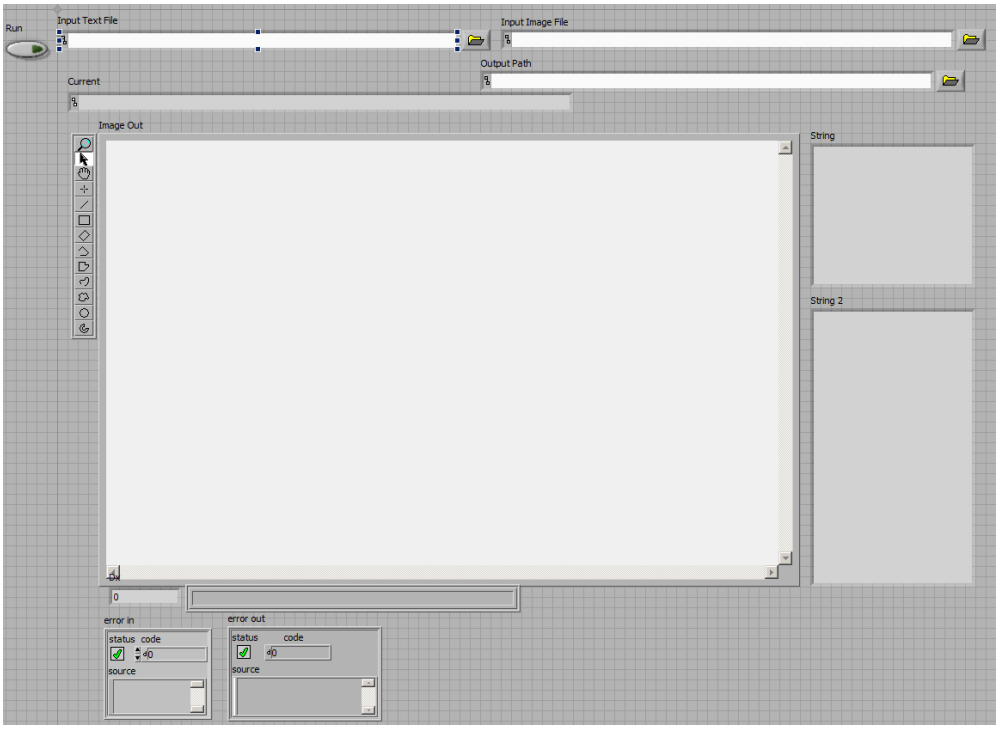

LabVeiw VI for Edge Detection Block Diagram

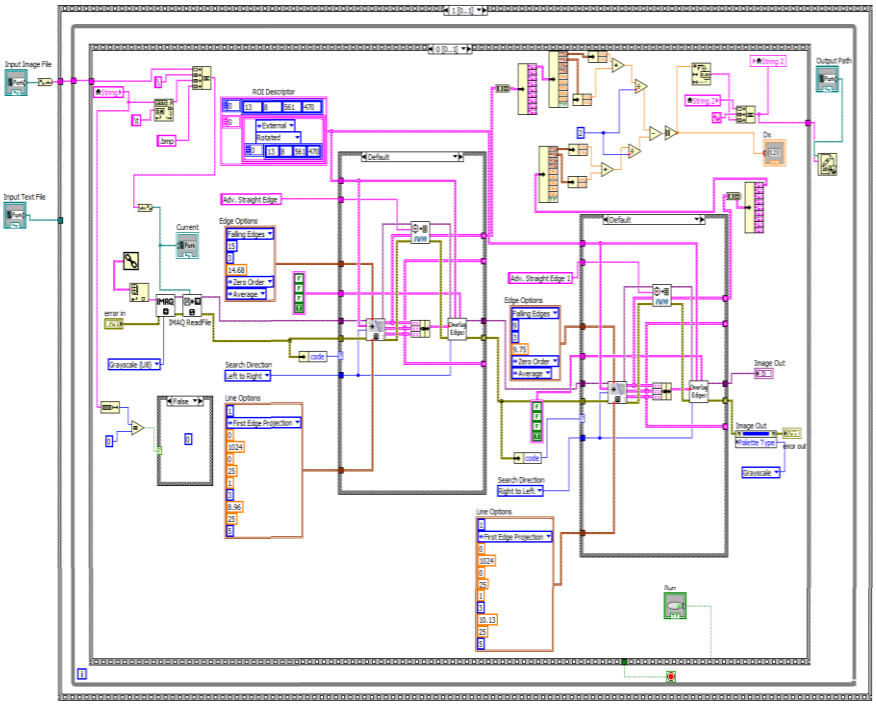

APPENDEX C

MATLAB Codes:

```
function [loc, co, R] = file1(Temp,Per,Press)
% expand will import excel files and fit a-b*exp(-c*t)
% imputs:
% output: i = inital width in pixels
%         max =  maximum expansion
%         tc = time constant(time it took to reach max)

%importing form Exel
Temp=[50 60];
Per=[100 80 60];
Press=[2000];

for T = 1:2;
   for P = 1:3;
      for S = 1:1;
      Temp1 = Temp(T);
      STemp = num2str(Temp1);

      Per1 = Per(P);
      SPer = num2str(Per1);

      Press1 = Press(S);
      SPress = num2str(Press1);

      filename = strcat(STemp, SPer, SPress,'.xlsx');
      fn=strcat(STemp, SPer, SPress);
      filepath = fullfile('C:', 'Users', 'Teng','desktop','DataAll', filename); %make file name

      x = xlsread(filepath,'d300:d7000');
      y = xlsread(filepath,'h300:h7000');

      y=smooth(x,y,81,'rlowess',3);
      figure('Numbertitle','off','Name',fn);
      z=plot(x,y);
      hold all;
      fo = fitoptions('method','NonlinearLeastSquares','Lower',[0 0 0]);

      st = [0 0 550];
      set(fo,'Startpoint',st);
      ft = fittype('-a*(exp(-b*x)+exp(-b*x*4)/4+exp(-b*x*9)/9+exp(-b*x*16)/16+exp(-
b*x*25)/25+exp(-b*x*36)/36+exp(-b*x*49)/49+exp(-b*x*64)/64+exp(-b*x*81)/81+exp(-
b*x*100)/100)+c',...
```

```
    'dependent',{'y'},'independent',{'x'},...
    'coefficients',{'a', 'b', 'c'});
        cf = fit(x,y,ft,fo);
        z = plot(cf,'fit',0.95);
        [cfun,gof] = fit(x,y,ft,fo);

        loc = filename
        co  = coeffvalues(cfun)
        R   = getfield(gof,'rsquare')

        disp('<><><><><><><><><><><><><><><><><><><><><><><><><><><><><><><><>');
        end
    end
end
```